

PGE₂ limits effector expansion of tumour-infiltrating stem-like CD8⁺ T cells

<https://doi.org/10.1038/s41586-024-07254-x>

Received: 22 May 2023

Accepted: 28 February 2024

Published online: 24 April 2024

Open access

 Check for updates

Sebastian B. Lacher^{1,12}, Janina Dörr^{2,12}, Gustavo P. de Almeida³, Julian Hönninger^{1,4}, Felix Bayerl¹, Anna Hirschberger¹, Anna-Marie Pedde¹, Philippa Meiser¹, Lukas Ramsauer¹, Thomas J. Rudolph¹, Nadine Spranger¹, Matteo Morotti^{5,6,7}, Alizee J. Grimm^{5,6,7}, Sebastian Jarosch^{4,11}, Arman Oner², Lisa Gregor², Stefanie Lesch², Stefanos Michaelides², Luisa Fertig², Daria Briukhovetska², Lina Majed², Sophia Stock^{2,8,9}, Dirk H. Busch⁴, Veit R. Buchholz⁴, Percy A. Knolle¹, Dietmar Zehn³, Denarda Dangaj Laniti^{5,6,7}, Sebastian Kobold^{2,9,10,13} & Jan P. Böttcher^{1,13}✉

Cancer-specific TCF1⁺ stem-like CD8⁺ T cells can drive protective anticancer immunity through expansion and effector cell differentiation^{1–4}; however, this response is dysfunctional in tumours. Current cancer immunotherapies^{2,5–9} can promote anticancer responses through TCF1⁺ stem-like CD8⁺ T cells in some but not all patients. This variation points towards currently ill-defined mechanisms that limit TCF1⁺CD8⁺ T cell-mediated anticancer immunity. Here we demonstrate that tumour-derived prostaglandin E₂ (PGE₂) restricts the proliferative expansion and effector differentiation of TCF1⁺CD8⁺ T cells within tumours, which promotes cancer immune escape. PGE₂ does not affect the priming of TCF1⁺CD8⁺ T cells in draining lymph nodes. PGE₂ acts through EP₂ and EP₄ (EP₂/EP₄) receptor signalling in CD8⁺ T cells to limit the intratumoural generation of early and late effector T cell populations that originate from TCF1⁺ tumour-infiltrating CD8⁺ T lymphocytes (TILs). Ablation of EP₂/EP₄ signalling in cancer-specific CD8⁺ T cells rescues their expansion and effector differentiation within tumours and leads to tumour elimination in multiple mouse cancer models. Mechanistically, suppression of the interleukin-2 (IL-2) signalling pathway underlies the PGE₂-mediated inhibition of TCF1⁺ TIL responses. Altogether, we uncover a key mechanism that restricts the IL-2 responsiveness of TCF1⁺ TILs and prevents anticancer T cell responses that originate from these cells. This study identifies the PGE₂–EP₂/EP₄ axis as a molecular target to restore IL-2 responsiveness in anticancer TILs to achieve cancer immune control.

Increased production of the bioactive lipid PGE₂ downstream of aberrant cyclooxygenase 1 (COX1; encoded by *Ptgs1*) and COX2 (encoded by *Ptgs2*) activity is observed in many human tumours and is associated with cancer progression and poor patient survival^{10–13}. Studies using preclinical mouse cancer models have demonstrated that tumour-derived PGE₂ has an important role in tumour escape from anticancer immunity^{14,15}. PGE₂ signalling is mediated by four G protein-coupled receptors that are broadly expressed on various immune cell populations, EP₁, EP₂, EP₃ and EP₄ (encoded by *PTGER1*, *PTGER2*, *PTGER3* and *PTGER4*, respectively), of which signalling through EP₂/EP₄ can suppress immune cell function¹⁶. Previous studies have implicated a role for PGE₂ in the regulation of T cell biology and function^{17–20}; however, the impact of PGE₂ on TCF1⁺CD8⁺ T cells

and their ability to mount protective anticancer responses remains unclear.

The PGE₂–EP₂/EP₄ axis controls anticancer CD8⁺ T cell responses

To determine the role of PGE₂ in tumour escape from anticancer T cell responses, we generated *Cd4^{cre}Ptger2^{-/-}Ptger4^{fl/fl}* mice in which Cre recombinase activity induces the deletion of EP₄ in CD4⁺ and CD8⁺ T cells on a global EP₂-deficient background. We also generated additional control mice that lack only EP₂ (*Ptger2^{-/-}Ptger4^{fl/fl}* mice), which enabled the testing of possible effects of global EP₂ deficiency. T cell profiling in *Cd4^{cre}Ptger2^{-/-}Ptger4^{fl/fl}* mice and *Ptger2^{-/-}Ptger4^{fl/fl}*

¹Institute of Molecular Immunology, School of Medicine and Health, Technical University of Munich (TUM), Munich, Germany. ²Division of Clinical Pharmacology, Department of Medicine IV, LMU University Hospital, Member of the German Center for Lung Research (DZL), LMU Munich, Munich, Germany. ³Division of Animal Physiology and Immunology, School of Life Sciences Weihenstephan, TUM, Freising, Germany. ⁴Institute for Medical Microbiology, Immunology and Hygiene, School of Medicine and Health, TUM, Munich, Germany. ⁵Ludwig Institute for Cancer Research, Lausanne Branch, University of Lausanne (UNIL), Lausanne, Switzerland. ⁶Department of Oncology, University Hospital of Lausanne (CHUV) and UNIL, Lausanne, Switzerland. ⁷Agora Cancer Research Center, Lausanne, Switzerland. ⁸Department of Medicine III, LMU University Hospital, LMU Munich, Munich, Germany. ⁹German Cancer Consortium (DKTK), partner site Munich, a partnership between DKFZ and LMU University Hospital, Munich, Germany. ¹⁰Einheit für Klinische Pharmakologie (EKLIP), Helmholtz Munich, Research Center for Environmental Health (HMGU), Neuherberg, Germany. ¹¹Present address: Boehringer Ingelheim, Biberach, Germany. ¹²These authors contributed equally: Sebastian B. Lacher and Janina Dörr. ¹³These authors jointly supervised this work: Sebastian Kobold and Jan P. Böttcher. ✉e-mail: j.boettcher@tum.de

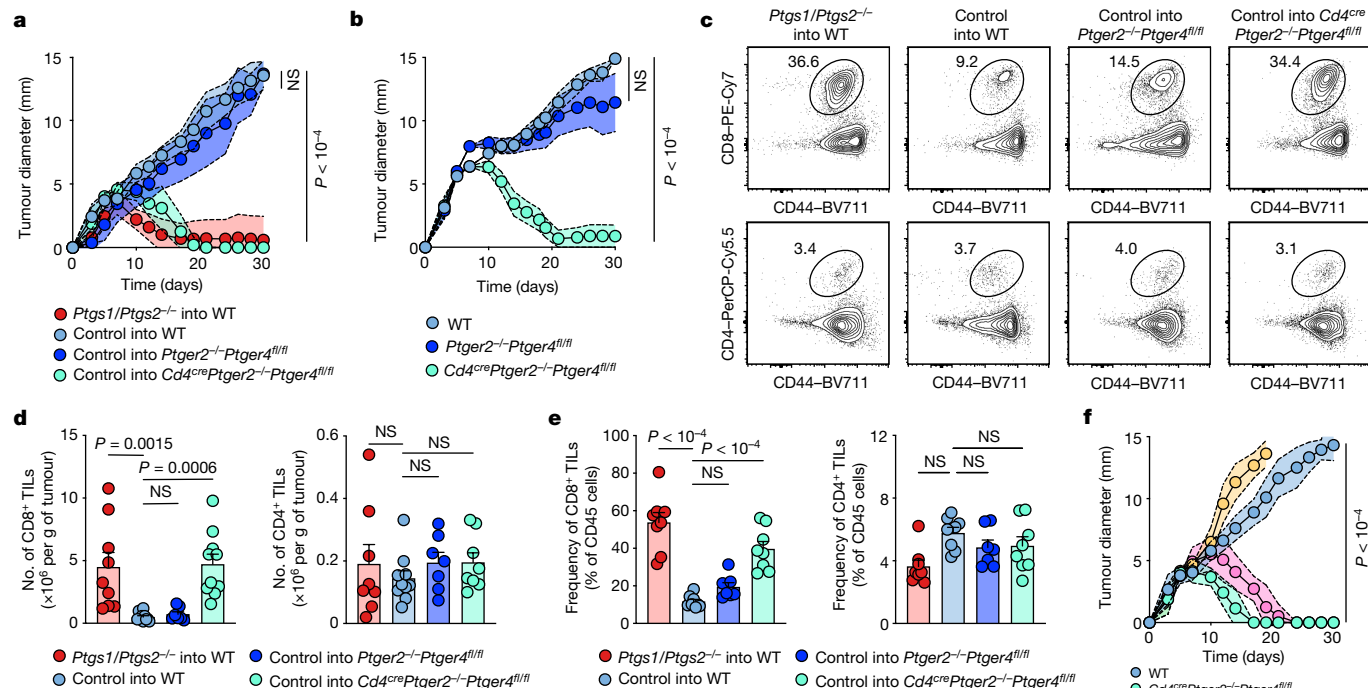


Fig. 1 | EP₂/EP₄ deficiency permits CD8⁺ T cell-mediated tumour immune control.

a, Tumour growth profiles of 2×10^5 *Ptgs1/Ptgs2^{-/-}* or control BRAF^{V600E} melanoma cells transplanted into WT mice, *Ptger2^{-/-}Ptger4^{fl/fl}* mice and *Cd4^{cre}Ptger2^{-/-}Ptger4^{fl/fl}* mice ($n = 10$ each). **b**, Growth profiles of 2×10^6 Panc02 cells transplanted into WT mice, *Ptger2^{-/-}Ptger4^{fl/fl}* mice and *Cd4^{cre}Ptger2^{-/-}Ptger4^{fl/fl}* mice ($n = 8$ each). **c–e**, WT mice, *Ptger2^{-/-}Ptger4^{fl/fl}* mice and *Cd4^{cre}Ptger2^{-/-}Ptger4^{fl/fl}* mice were subcutaneously (s.c.) injected with 2×10^6 control or *Ptgs1/Ptgs2^{-/-}* BRAF^{V600E} cells and TILs were analysed 11 days later by flow cytometry. **c**, Plots showing the frequencies of CD8⁺ and CD4⁺ TILs among CD45⁺ immune cells and expression of the activation marker CD44. **d**, Quantification of TIL numbers (CD8⁺ TILs: *Ptgs1/Ptgs2^{-/-}* into WT, $n = 9$; control into WT, $n = 10$; control into *Ptger2^{-/-}Ptger4^{fl/fl}*, $n = 7$; control into

Cd4^{cre}Ptger2^{-/-}Ptger4^{fl/fl}, $n = 10$; CD4⁺ TILs: *Ptgs1/Ptgs2^{-/-}* into WT, $n = 8$; control into WT, $n = 10$; control into *Ptger2^{-/-}Ptger4^{fl/fl}*, $n = 7$; control into *Cd4^{cre}Ptger2^{-/-}Ptger4^{fl/fl}*, $n = 8$). **e**, TIL frequencies (*Ptgs1/Ptgs2^{-/-}* into WT, $n = 8$; control into WT, $n = 8$; control into *Ptger2^{-/-}Ptger4^{fl/fl}*, $n = 7$; control into *Cd4^{cre}Ptger2^{-/-}Ptger4^{fl/fl}*, $n = 8$). **f**, Effect of CD8⁺ and CD4⁺ T cell depletion on control BRAF^{V600E} tumour growth in *Cd4^{cre}Ptger2^{-/-}Ptger4^{fl/fl}* mice (*Cd4^{cre}Ptger2^{-/-}Ptger4^{fl/fl}*, $n = 8$; WT, $n = 9$). Data in **a**, **b** and **d–f** are pooled from two (**b**, **f**) or three (**a**, **d**, **e**) independent experiments and depicted as the mean \pm s.e.m. Plots in **c** show data for 1 tumour representative of $n = 7$ tumours from 2 independent experiments. *P* values are from two-way analysis of variance (ANOVA) with Bonferroni's correction for multiple testing (**a**, **b**, **f**) or one-way ANOVA with Dunnett's multiple-comparison test (**d**, **e**). NS, not significant ($P \geq 0.05$).

mice compared with C57BL/6 wild-type (WT) mice revealed normal CD4⁺ and CD8⁺ T cell abundance and subset composition in lymphoid organs (Extended Data Fig. 1a–g). Unaltered T cell composition was similarly observed in *Gzmb^{cre}Ptger2^{-/-}Ptger4^{fl/fl}* mice, which lack EP₂ and EP₄ in CD8⁺ T cells expressing granzyme B (GZMB) (Extended Data Fig. 1a–g). Notably, after tumour challenge, *Cd4^{cre}Ptger2^{-/-}Ptger4^{fl/fl}* mice exhibited improved tumour immune control, and fully rejected tumours formed by immune-evasive, PGE₂-producing (control) BRAF^{V600E} melanoma cells (Fig. 1a and Extended Data Fig. 2a). This was not the case for *Ptger2^{-/-}Ptger4^{fl/fl}* mice and WT mice, in which control BRAF^{V600E} tumours progressively grew (Fig. 1a and Extended Data Fig. 2a). We further validated that BRAF^{V600E} melanoma depended on tumour-derived PGE₂ to evade anticancer immunity by demonstrating that COX-deficient *Ptgs1/Ptgs2^{-/-}* BRAF^{V600E} melanoma, which lacks PGE₂ production, failed to escape immune control (Fig. 1a and Extended Data Fig. 2a). We also confirmed that this effect is mediated by CD8⁺ T cells¹⁴ (Extended Data Fig. 2b). Extending our analysis to other mouse tumour models, tumours formed by Panc02 pancreatic cancer cells similarly exhibited complete regression in *Cd4^{cre}Ptger2^{-/-}Ptger4^{fl/fl}* mice but not in *Ptger2^{-/-}Ptger4^{fl/fl}* or WT mice (Fig. 1b and Extended Data Fig. 2c). Similar results were observed for tumours derived from MC38 colorectal cancer cells (Extended Data Fig. 2d,e).

Immune control of control BRAF^{V600E} melanoma tumours in *Cd4^{cre}Ptger2^{-/-}Ptger4^{fl/fl}* mice was linked to markedly increased CD8⁺ TIL accumulation (Fig. 1c–e). By contrast, no substantial differences

were observed for CD4⁺ TILs (Fig. 1c–e). This result suggests that although PGE₂–EP₂/EP₄ signalling may affect CD4⁺ T cell function, these cells, at least in BRAF^{V600E} tumours, do not have a major role in immune escape. Consistently, antibody-mediated T cell depletion confirmed the relevance of CD8⁺ but not CD4⁺ T cells for immune control of PGE₂-producing BRAF^{V600E} tumours in *Cd4^{cre}Ptger2^{-/-}Ptger4^{fl/fl}* mice (Fig. 1f). Taken together, these data suggest that EP₂/EP₄ signalling controls the accumulation of CD8⁺ TILs in PGE₂-producing tumours and that this is important for cancer immune evasion.

PGE₂ does not affect CD8⁺ T cell priming

Priming of anticancer CD8⁺ T cells in tumour-draining lymph nodes (tdLNs) by type 1 conventional dendritic cells (cDC1s) that transport tumour antigens to tdLNs is thought to underlie anticancer CD8⁺ T cell responses^{21,22}. To test whether PGE₂ impairs cDC1-mediated CD8⁺ T cell priming, we injected WT mice with PGE₂-producing control or PGE₂-deficient *Ptgs1/Ptgs2^{-/-}* BRAF^{V600E} melanoma cells engineered to express the model antigen ovalbumin (OVA). We then determined the presence of migratory CD103⁺ cDC1 cross-presenting OVA-derived peptides on major histocompatibility complex (MHC) class I molecules in tdLNs (Extended Data Fig. 3a). Migratory cDC1s in both models cross-presented tumour-derived OVA protein with similar efficiency, as determined by staining for OVA(257–264) (SIINFEKL) peptide loading of the MHC class I molecule H-2K^b (Extended Data Fig. 3b,c).

To further examine T cell priming, we adoptively transferred naive CD8⁺ OT-I T cells (Extended Data Fig. 3d), which express a transgenic T cell receptor (TCR) specific for OVA, into mice subsequently transplanted with BRAF^{V600E}-OVA tumours. Naive (CD44^{low}) OT-I T cells efficiently expanded into CD44⁺TCF1⁺ OT-I T cells within tDLNs in both groups (Extended Data Fig. 3e,f). This result demonstrates that T cell priming is unaffected. Consistent with these data, we did not detect substantial PGE₂ levels in tDLNs from control BRAF^{V600E} tumours or in other distant organs (Extended Data Fig. 3g). Moreover, progressive outgrowth of control BRAF^{V600E} tumours and efficient immune control of *Ptgs1/Ptgs2*^{-/-} BRAF^{V600E} tumours was unchanged following tumour transplantation to the same lymph drainage site (Extended Data Fig. 3h). These findings imply that an anticancer CD8⁺ T cell response initiated in the shared tDLN achieves effective elimination of the PGE₂-deficient tumour but nevertheless fails in the co-transplanted PGE₂-producing tumour. Taken together, these data demonstrate that PGE₂ controls anticancer CD8⁺ T cell responses locally within tumour tissue, which raises the question of how it affects CD8⁺ TILs.

PGE₂ controls CD8⁺ TIL effector expansion

CD8⁺ TILs are heterogenous and comprise at least two phenotypically and functionally distinct populations: (1) proliferation and differentiation competent TCF1⁺ cells that lack cytotoxic effector functions (often referred to as 'stem-like' or 'precursor of exhausted' T cells); and (2) TIM-3⁺(TCF1⁻) cells that encompass more differentiated effector and terminally differentiated or exhausted T cells. TCF1⁺CD8⁺ T cells fulfil an essential role in anticancer immunity by giving rise to TIM-3⁺ progeny through proliferative expansion and effector differentiation^{2,5,8,9}. This process is pivotal for anticancer immunity that at least in part occurs locally within tumour tissue¹⁻³.

Our results raised the question of whether interference with effector differentiation of TCF1⁺CD8⁺ TILs underlies the PGE₂-mediated impairment of anticancer immunity. To address this issue across the single-cell landscape of CD8⁺ TILs, we performed parallel single-cell RNA sequencing (scRNA-seq) and single-cell TCR sequencing (scTCR-seq) of CD8⁺ TILs sorted from BRAF^{V600E} tumours at day 11 after tumour transplantation into *Cd4^{cre}Ptger2^{-/-}Ptger4^{fl/fl}* mice and *Ptger2^{-/-}Ptger4^{fl/fl}* mice (as control) (Fig. 2a and Extended Data Fig. 4a). We also included *Gzmb^{cre}Ptger2^{-/-}Ptger4^{fl/fl}* mice (Fig. 2a), reasoning that this would enable us to determine the impact of EP₂/EP₄-mediated PGE₂ signalling on those CD8⁺ T cells undergoing effector differentiation within tumour tissue. We further included four biological replicates in each group to ensure that heterogeneity among individual tumours is reflected in our analysis. scRNA-seq analysis revealed eight TIL clusters (Fig. 2b) that all expressed *Pdcd1* (which encodes PD-1), the activation marker *Cd44* and the transcription factor (TF) *Tox* (Extended Data Fig. 4b), a result consistent with their activation history. Of note, CD8⁺ TILs displayed equally high protein expression of CD44, TOX and PD-1 that did not differ among cells isolated from tumours in *Ptger2^{-/-}Ptger4^{fl/fl}* mice, *Cd4^{cre}Ptger2^{-/-}Ptger4^{fl/fl}* mice and *Gzmb^{cre}Ptger2^{-/-}Ptger4^{fl/fl}* mice (Extended Data Fig. 4c).

In our concatenated scRNA-seq data, TIL clusters 1 and 2 shared high expression of stem-like T cell markers such as *Tcf7* (which encodes TCF1), *Slamf6* and *Il7r* (Fig. 2c,d and Extended Data Fig. 4d). Of note, both of these clusters displayed markedly higher expression of gene signatures of memory or tumour-reactive T cells than signatures for naive T cells (Extended Data Fig. 4e,f), which indicated that at least a substantial fraction of these cells is antigen-experienced. TCF1⁺ TILs in cluster 1 displayed enriched expression of *Sell* (which encodes CD62L), *Ccr7* and *Bach2* (Extended Data Fig. 4d,g,h). By contrast, TCF1⁺ TILs in cluster 2 lacked *Sell* but showed expression of markers associated with effector function (such as *Gzmb*, *Gzmk* and *Fasl*) and migration (*S1pr1*, *Itga4*, *Gpr183*, *Itgb1*, *Cxcr3* and *Ier2*) (Fig. 2d and Extended Data Fig. 4d,g,h), which indicated their incipient effector differentiation.

Consistently, CD62L⁺TCF1⁺ TILs but not CD62L⁻TCF1⁺ TILs stained positive for intracellular GZMB protein (Extended Data Fig. 4i), although GZMB expression in these cells was low both in terms of frequency of GZMB⁺ cells and total GZMB levels. The remaining scRNA-seq clusters (clusters 3–8) lacked *Tcf7* expression and, in addition to *Gzmb*, shared expression of genes associated with T cell differentiation and effector function, including *Havcr2* (which encodes TIM-3) and high expression of the chemokine receptor *Cxcr6* (Fig. 2c,d and Extended Data Fig. 4g,h), which identified them as more differentiated early and/or terminally differentiated TIL populations. We confirmed co-expression of TIM-3 and CXCR6 at the protein level (Extended Data Fig. 4j) and used both molecules as overarching markers to collectively denote (TCF1⁻) effector TILs. Among the different clusters of TIM-3⁺CXCR6⁺ TILs, clusters 3 and 4 were marked by high expression of molecules associated with early effector-like cells; for example, *Cx3cr1* (refs. 23,24) in cluster 3 and *Cd7* (ref. 25) in cluster 4 (Extended Data Fig. 4d,h). By contrast, clusters 5–8 displayed increased expression of cytotoxic effector molecules and immune-inhibitory receptors (Fig. 2d and Extended Data Fig. 4h), but were distinguished by differential expression of cytokines (for example, *Ifng* and *Tnf*), molecules associated with growth arrest and DNA repair (*Apex1* and *Gadd45b*) and type I interferon signalling (*Isg15*, *Ifit1* and *Ifit3*) (Extended Data Fig. 4d,h). Notably, in contrast to tumour tissue, we did not detect any GZMB⁺ cells among activated CD44⁺CD8⁺ T cells in tDLNs or spleen of tumour-bearing mice (Extended Data Fig. 4k). This result supports the notion that effector differentiation of anticancer CD8⁺ T cells occurs within tumour tissue. Unsupervised slingshot analysis of our TIL scRNA-seq data uncovered a tree-shaped developmental trajectory that begins with TCF1⁺ cells and progresses over CX₃CR1^{hi}TIM-3⁺ effector cells into CD7^{hi}TIM-3⁺ effector cells, from which it branches off into distinct terminally differentiated T cell populations (Fig. 2e). Together, these results indicate a progressive trajectory for TIL differentiation within tumours that originates from TCF1⁺ TILs and follows a unidirectional path of effector differentiation before ending in multiple smaller branches of terminally differentiated TIL populations.

To assess the impact of PGE₂-EP₂/EP₄ signalling on the landscape of CD8⁺ TILs, we separated our scRNA-seq data on the basis of recipient mouse groups. Density analysis revealed a prominent shift towards early effector (clusters 3 and 4) and terminally differentiated TIL populations (cluster 5) in both *Cd4^{cre}Ptger2^{-/-}Ptger4^{fl/fl}* mice and *Gzmb^{cre}Ptger2^{-/-}Ptger4^{fl/fl}* mice compared with *Ptger2^{-/-}Ptger4^{fl/fl}* mice (Fig. 2f). We therefore quantified the frequencies TIL populations across all replicates. *Ptger2^{-/-}Ptger4^{fl/fl}* mice lacked expansion of any differentiating effector TIL populations (Fig. 2g). By contrast, in *Cd4^{cre}Ptger2^{-/-}Ptger4^{fl/fl}* mice, we detected elevated frequencies of early and late effector TIL populations that further increased progressively along the common trajectory of effector differentiation (clusters 2–5; Fig. 2g). This pattern was similarly observed for *Gzmb^{cre}Ptger2^{-/-}Ptger4^{fl/fl}* mice (Fig. 2g), in which TIL expansion was even more prominent, which probably reflects additional favourable activity of intratumoural GZMB⁺ natural killer cells¹⁵. Enhanced TIL expansion in *Cd4^{cre}Ptger2^{-/-}Ptger4^{fl/fl}* mice and *Gzmb^{cre}Ptger2^{-/-}Ptger4^{fl/fl}* mice correlated with the fact that TCF1⁺ and TIM-3⁺CXCR6⁺ TILs in both models had lost *Ptger2* and *Ptger4* expression (Extended Data Fig. 5a–d). Consistent with the notion that intratumoural effector differentiation causes the loss of EP₄ in TCF1⁺ TILs in *Gzmb^{cre}Ptger2^{-/-}Ptger4^{fl/fl}* mice, *Gzmb^{cre}Ptger2^{-/-}Ptger4^{fl/fl}* TCF1⁺CD8⁺ T cells generated in vitro displayed efficient *Ptger4* ablation in an effector differentiation assay (Extended Data Fig. 5e,f). In line with enhanced TIL expansion, expression of a proliferation signature in effector TIL populations from *Cd4^{cre}Ptger2^{-/-}Ptger4^{fl/fl}* mice and *Gzmb^{cre}Ptger2^{-/-}Ptger4^{fl/fl}* mice was higher than from *Ptger2^{-/-}Ptger4^{fl/fl}* mice (Extended Data Fig. 5g). Consistently, EP₂/EP₄-deficient TCF1⁺ TILs and their TIM-3⁺ progeny displayed increased expression of the proliferation marker Ki-67 (Extended Data Fig. 5h). However, we did not detect a substantial gain in expression of a gene signature for cytotoxic

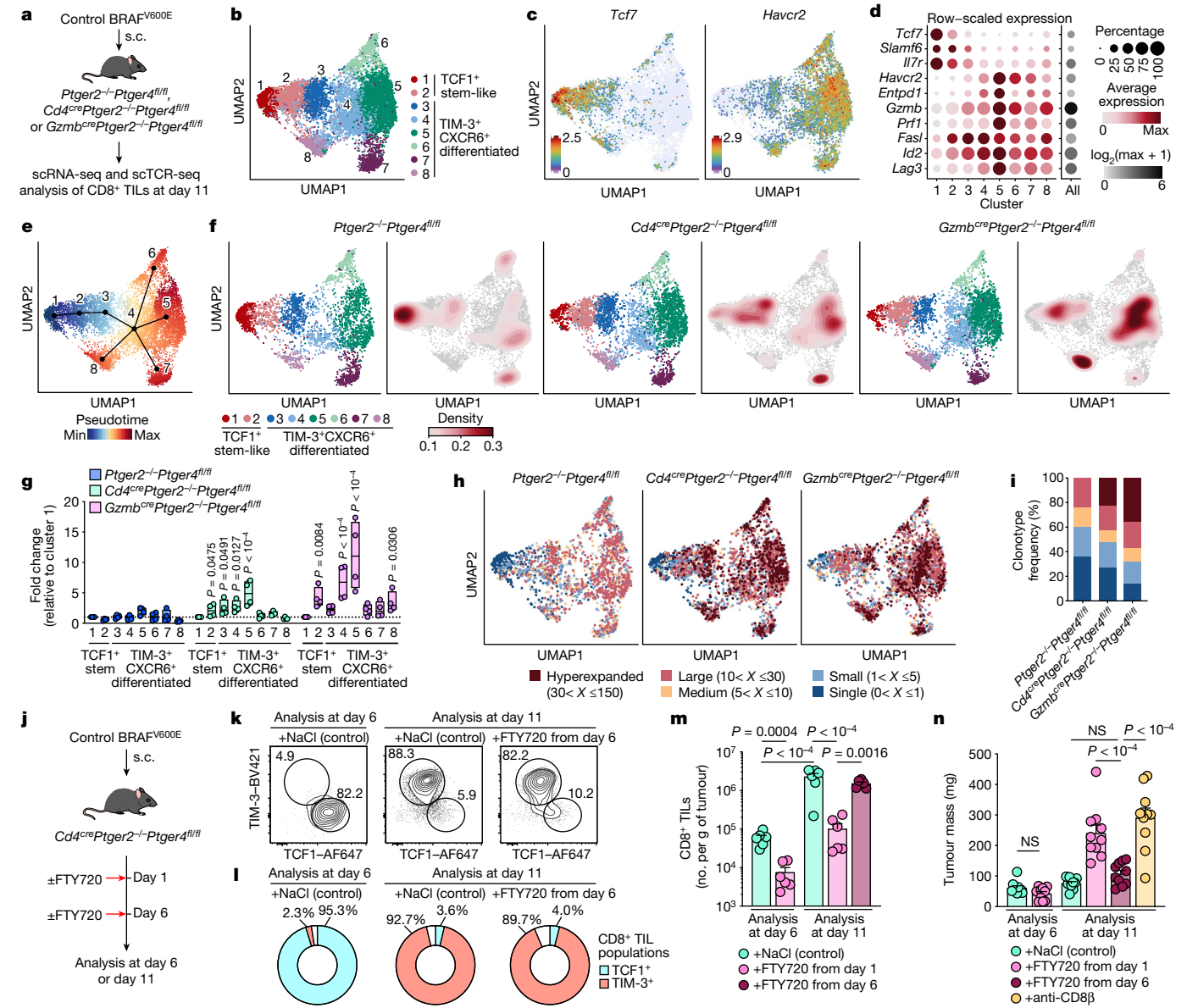


Fig. 2 | Ablation of T cell-intrinsic EP₂/EP₄ signalling rescues CD8⁺ T cell expansion and effector differentiation in PGE₂-producing tumours. **a–g**, scRNA-seq analyses of CD8⁺ TILs in control BRAF^{V600E} tumours from *Ptger2*^{-/-}*Ptger4*^{fl/fl} mice, *Cd4*^{cre}*Ptger2*^{-/-}*Ptger4*^{fl/fl} mice and *Gzmb*^{cre}*Ptger2*^{-/-}*Ptger4*^{fl/fl} mice (*n* = 4 each). **a**, Experimental design. **b**, Uniform manifold approximation and projection (UMAP) plot of 12,516 CD8⁺ TILs coloured according to cluster classification. **c**, Visualization of *Tcf7* and *Havcr2* transcript levels. **d**, PCPT plot showing expression levels of selected genes. **e**, Developmental trajectory prediction by unsupervised slingshot analysis. **f, g**, Comparison of CD8⁺ TIL clusters among *Ptger2*^{-/-}*Ptger4*^{fl/fl} mice, *Cd4*^{cre}*Ptger2*^{-/-}*Ptger4*^{fl/fl} mice and *Gzmb*^{cre}*Ptger2*^{-/-}*Ptger4*^{fl/fl} mice. **f**, Density analysis. **g**, Quantification relative to cluster 1 (*n* = 4 each). **h, i**, scTCR-seq analyses of CD8⁺ TILs from *n* = 3 tumours for each group. **h**, UMAP visualizations of T cell clonotype distribution. **i**, Quantification of T cell clonotype frequency. **j–n**, TIM-3⁺ effector CD8⁺ T cell differentiation in tumour tissue. *Cd4*^{cre}*Ptger2*^{-/-}*Ptger4*^{fl/fl} mice bearing control

BRAF^{V600E} tumours were injected with FTY720 or NaCl as control. **j**, Experimental design. **k**, Representative flow cytometry plots showing TCF1 and TIM-3 expression among CD44⁺CD8⁺ TILs. **l**, Average percentage of CD8⁺ TIL populations across *n* = 6 tumours. **m**, Quantification of CD8⁺ TIL numbers (*n* = 6). **n**, Analysis of tumour mass (*n* = 10). Anti-CD8 β antibody-mediated CD8⁺ T cell depletion in the absence of FTY720 treatment. Data in **a–h** are from one experiment. Data in **g** are depicted as box plots extending from the 25th to 75th percentiles with the median as the centre and the whiskers corresponding to the minimum and maximum values. Data in **k–n** are pooled from two (**k, l, m**) or three (**n**) independent experiments and depicted as the mean \pm s.e.m. *P* values are from two-way ANOVA with Bonferroni's correction for multiple testing (**g**) or one-way ANOVA with Tukey's multiple-comparison test (**m, n**). Plots in **k** show data for 1 tumour representative for *n* = 6 tumours from 2 independent experiments.

effector function in these TIL populations (Extended Data Fig. 5i). Thus, PGE₂ does not modify the expression of genes associated with T cell function but prevents their differentiation and expansion, which highlights a mechanistic difference to canonical factors that drive dysfunctional CD8⁺ T cell responses through transcriptional programming, such as TOX^{26,27} or MYB²⁸. Taken together, these findings suggest that tumour-derived PGE₂ locally impairs the differentiation and expansion

of effector T cell populations arising from TCF1⁺ TILs. Moreover, EP₂/EP₄ deficiency rescues TILs from this inhibitory effect of PGE₂.

PGE₂-EP₂/EP₄ signalling limits clonal TIL expansion
Analyses of our scTCR-seq data revealed that many CD8⁺ TILs consisted of clonally expanded cells (Extended Data Fig. 6a–c), which

is an indicator of tumour specificity and proliferative T cell expansion^{29,30}. Notably, although expanded clonotypes were detectable in all TIL populations, they were more prominent among TIM-3⁺CXCR6⁺ cells (clusters 3–8) (Extended Data Fig. 6a–c), a result consistent with the notion that these differentiated TIL populations may arise locally through the proliferative expansion of a few tumour-specific TCF1⁺ TILs. Moreover, highly expanded TIL clones (>30) were completely absent from tumours in *Ptger2*^{-/-}*Ptger4*^{fl/fl} mice but were abundant in both *Cd4*^{cre}*Ptger2*^{-/-}*Ptger4*^{fl/fl} mice (22.6%) and *Gzmb*^{cre}*Ptger2*^{-/-}*Ptger4*^{fl/fl} mice (35.6%) (Fig. 2h,i and Extended Data Fig. 6d). Consistently, *Ptger2*^{-/-}*Ptger4*^{fl/fl} mice displayed an increased frequency of poorly expanded small or single clones (Fig. 2h,i and Extended Data Fig. 6d). Notably, TILs in both *Cd4*^{cre}*Ptger2*^{-/-}*Ptger4*^{fl/fl} mice and *Gzmb*^{cre}*Ptger2*^{-/-}*Ptger4*^{fl/fl} mice had much higher fractions of clones shared between TCF1⁺ cells and TIM-3⁺CXCR6⁺ effector progeny (9.1% and 14.5%, respectively) than *Ptger2*^{-/-}*Ptger4*^{fl/fl} mice (3.9%) (Extended Data Fig. 6e). The few shared clones detectable in *Ptger2*^{-/-}*Ptger4*^{fl/fl} mice, however, only showed poor expansion (Extended Data Fig. 6f). We conclude that tumour-derived PGE₂ restricts clonal TIL expansion, which results in a collapse of the intratumoural CD8⁺ T cell response. This impairment is overcome by ablation of EP₂/EP₄ in CD8⁺ T cells, which leads to the productive differentiation and expansion of clonal effector T cell progeny within tumour tissue.

TCF1⁺ TIL effector expansion achieves tumour control

We next sought to provide further evidence that EP₂/EP₄ deficiency in CD8⁺ T cells permits productive effector differentiation of TILs in PGE₂-producing tumours. Quantification of TIL populations across PGE₂-deficient *Ptgs1*/*Ptgs2*^{-/-} BRAF^{V600E} tumours from WT mice and PGE₂-producing control BRAF^{V600E} from WT mice, *Ptger2*^{-/-}*Ptger4*^{fl/fl} mice and *Cd4*^{cre}*Ptger2*^{-/-}*Ptger4*^{fl/fl} mice (Extended Data Fig. 7a–c) revealed that the numbers of TCF1⁺ TILs were comparable among all groups (Extended Data Fig. 7b). This result indicated that the generation of TCF1⁺CD8⁺ T cells in lymphoid tissues and their tumour infiltration is not affected by PGE₂. However, whereas the numbers of differentiated TIM-3⁺ TILs were low in control BRAF^{V600E} tumours in WT mice and *Ptger2*^{-/-}*Ptger4*^{fl/fl} mice, they were highly abundant in *Cd4*^{cre}*Ptger2*^{-/-}*Ptger4*^{fl/fl} mice (Extended Data Fig. 7c) and indistinguishable from those found in *Ptgs1*/*Ptgs2*^{-/-} BRAF^{V600E} tumours in WT mice.

To determine whether TIM-3⁺ TILs were generated from TCF1⁺ TILs locally within tumour tissue, we made use of our finding that at early stages after implantation (day 6), tumours contain TCF1⁺ TILs but not (yet) differentiated TIM-3⁺ TILs (Fig. 2j–n). Tumour-bearing *Cd4*^{cre}*Ptger2*^{-/-}*Ptger4*^{fl/fl} mice treated from day 6 onwards with the SIP1R antagonist FTY720, which prevents lymph node (LN) egress of newly primed CD8⁺ T cells³¹, showed unabated intratumoural development and prominent expansion of TIM-3⁺ TILs over time (Fig. 2k–m). By contrast, when initial tumour infiltration of TCF1⁺CD8⁺ T cells was blocked by FTY720 application from day 1 onwards, no intratumoural TIL expansion was detected (Fig. 2m). Notably, the proliferative response originating from TCF1⁺ TILs present in tumour tissue at day 6 was sufficient to achieve control of tumour growth (Fig. 2n). This result demonstrates that TCF1⁺ TILs locally generate potent anticancer effector responses when protected from inhibitory PGE₂ signalling in tumours.

PGE₂ suppresses IL-2 responsiveness of TILs

In an effort to identify the mechanisms downstream of PGE₂-EP₂/EP₄ signalling that determine impaired TIL responses, we performed TF activity analysis of our scRNA-seq data. Deficiency of EP₂/EP₄ in TCF1⁺ TILs resulted in an increased activity of TFs associated with effector differentiation (including NFKB1, REL, JUN and TBX21), stimulatory cytokine signalling (STAT4, IRF1, NFKB1, JUN and TBX21) and survival (RUNX2 and TRP53) (Fig. 3a and Extended Data Fig. 8a,b). Most of

these alterations were detectable in both TCF1⁺ TILs and their developing progeny (Extended Data Fig. 8c) and were highly consistent across *Cd4*^{cre}*Ptger2*^{-/-}*Ptger4*^{fl/fl} mice and *Gzmb*^{cre}*Ptger2*^{-/-}*Ptger4*^{fl/fl} mice (Fig. 3a and Extended Data Fig. 8c,d). Notably, we detected increased TF activity linked to IL-2 cytokine signalling (including STAT1, STAT3, STAT5B, ELK1 and NFATC2)³² in TILs from *Cd4*^{cre}*Ptger2*^{-/-}*Ptger4*^{fl/fl} mice and *Gzmb*^{cre}*Ptger2*^{-/-}*Ptger4*^{fl/fl} mice (Fig. 3a and Extended Data Fig. 8a,b). This result was again observed in both TCF1⁺ TILs and their TIM-3⁺CXCR6⁺ progeny (Extended Data Fig. 8c,d). PGE₂ may therefore affect the response of TILs to IL-2, which is a notable finding given the current development of new classes of IL-2 receptor (IL-2R) agonists for cancer therapy and the emerging role of IL-2 signalling for productive anticancer responses by TCF1⁺ TILs^{33,34}.

We therefore tested whether PGE₂ controls the IL-2-mediated expansion of TCF1⁺ TILs sorted from PGE₂-deficient *Ptgs1*/*Ptgs2*^{-/-} tumours (identified as TIM-3⁺CXCR6⁺ TILs; Extended Data Fig. 8e). PGE₂ strongly compromised the capacity of TCF1⁺ TILs to expand and differentiate into effector cells when stimulated with high-dose IL-2 together with anti-CD3 and anti-CD28 (anti-CD3/CD28) treatment^{35,36} (Fig. 3b). Bypassing the scarcity of TIL numbers, we further addressed this issue using antigen-experienced, repetitively activated TCF1⁺CD8⁺ T cells generated in vitro, on which PGE₂ had an identical inhibitory effect (Fig. 3c). In line with PGE₂-mediated impairment of IL-2-driven proliferation and effector differentiation, PGE₂-treated TCF1⁺CD8⁺ T cells from in vitro T cell cultures showed markedly reduced DNA replication early after their stimulation (Fig. 3d). Transcriptional profiling by RNA-seq (Fig. 3e) revealed that PGE₂ exposure resulted in distinct transcriptional changes in stimulated TCF1⁺CD8⁺ T cells and their unstimulated counterparts (Fig. 3f). Analyses of the stimulated T cell populations identified 294 differentially expressed genes (DEGs) following PGE₂ exposure (Fig. 3g). PGE₂-treated TCF1⁺CD8⁺ T cell populations expressed increased levels of transcripts encoding for molecules related to EP₂/EP₄-mediated cAMP signalling (*Crem* and *Fosl2*) and T cell quiescence (for example, *Phlpp1*, *Klf3* and *Klf4*) (Fig. 3g and Extended Data Fig. 8f). Gene set enrichment analysis (GSEA) showed a selective downregulation of the T cell differentiation-associated mTORC1 signalling pathway and the IL-2 signalling pathway (Fig. 3h). The latter result is consistent with the observed reduced IL-2 pathway activity in TILs identified in our scRNA-seq analysis and further supports the notion that PGE₂ impairs the proliferative expansion of TILs through the inhibition of IL-2 signalling.

In line with an inhibitory effect of PGE₂ on IL-2 signalling, IL-2 stimulation failed to promote STAT5 phosphorylation (pSTAT5) in PGE₂-treated TCF1⁺CD8⁺ T cells (Fig. 3i). Notably, this defect was associated with reduced surface expression of the IL-2R gamma chain (IL-2R γ c) (Extended Data Fig. 8g) and could only partially be rescued by stimulation with high doses of IL-2 (Fig. 3j). This result points towards a dominant inhibitory effect of PGE₂ on IL-2 signalling through the regulation of IL-2R γ c expression. Consistent with this notion, PGE₂ impaired the expansion of TCF1⁺CD8⁺ T cells not only in response to IL-2 but also the γ c cytokines IL-7 and IL-15 (Fig. 3k). Thus, PGE₂ fundamentally affects the entire γ c cytokine signalling pathway in TCF1⁺CD8⁺ T cells and their differentiating progeny. IL-2-mediated pSTAT5 (Fig. 3l,m) and IL-2-dependent T cell proliferation and expansion (Fig. 3n and Extended Data Fig. 8h,i) was rescued in TCF1⁺CD8⁺ T cells from *Cd4*^{cre}*Ptger2*^{-/-}*Ptger4*^{fl/fl} mice, which demonstrates the functional relevance of EP₂/EP₄ signalling for the restriction of IL-2 signalling. Taken together, these data suggest that the PGE₂-EP₂/EP₄ axis limits productive anticancer TIL responses by suppressing the IL-2 signalling pathway.

EP₂/EP₄-deficient TILs mediate cancer elimination

To examine antigen-specific TIL responses in more detail, we used WT (EP₂/EP₄-proficient) and *Cd4*^{cre}*Ptger2*^{-/-}*Ptger4*^{fl/fl} (EP₂/EP₄-deficient) OT-I T cells. We co-transferred a small number (1 × 10³ cells) of congenically

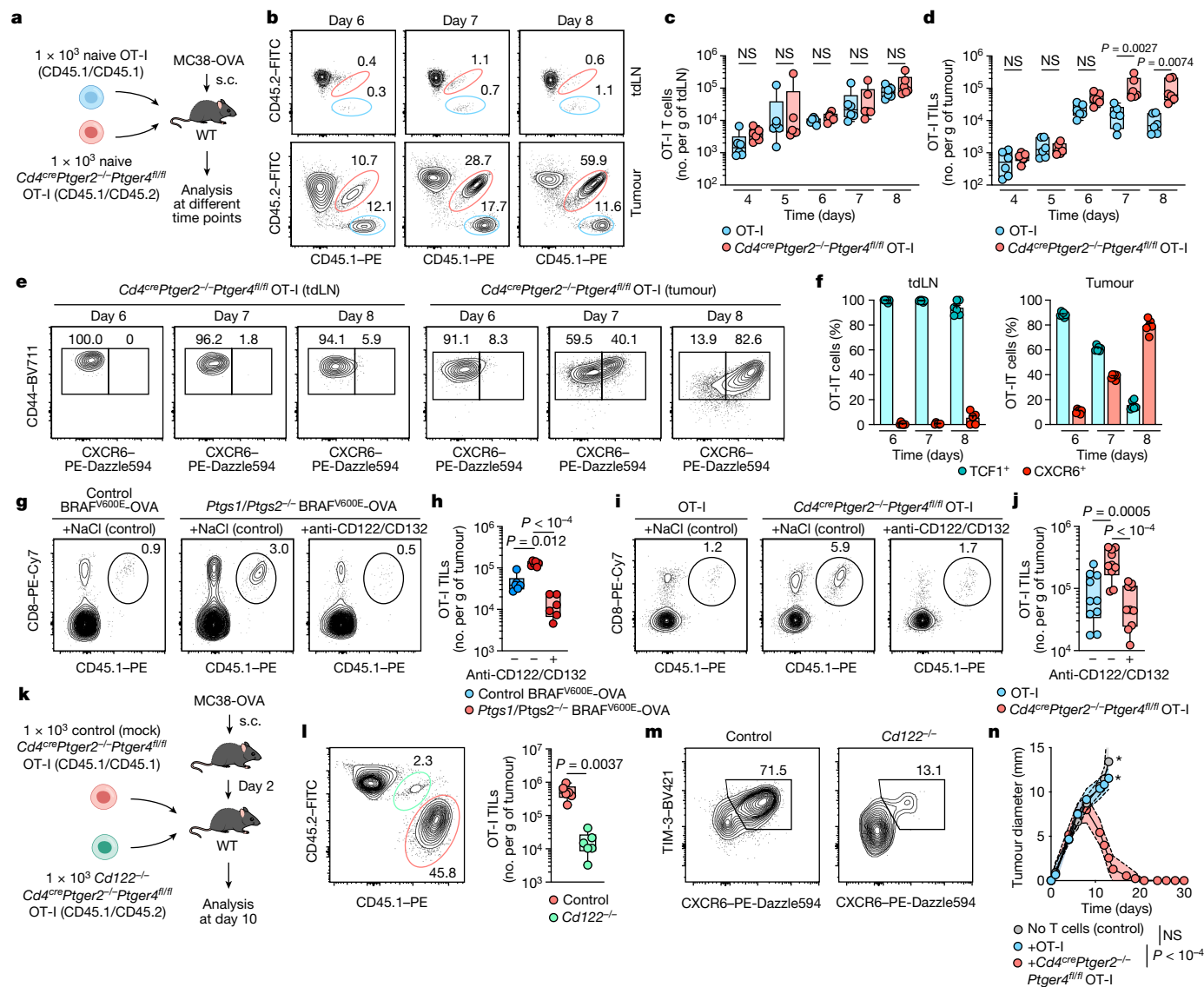


Fig. 4 | EP₂/EP₄-deficient tumour antigen-specific CD8⁺ T cells expand in PGE₂-producing tumours and mediate tumour immune control.

a, Experimental design for **b-f**. **b**, Flow cytometric plots of CD8⁺ T cells from tdLNs and tumours from the indicated days. **c,d**, Numbers of expanded OT-I CD8⁺ T cells in tdLNs (**c**) and tumours (**d**) at indicated time points ($n = 6$). **e,f**, Analysis of CD44 and CXCR6 expression in $Cd4^{cre}Ptger2^{-/-}Ptger4^{fl/fl}$ OT-I cells. **e**, Flow cytometry plots. **f**, Subset frequencies ($n = 6$). **g-j**, Effect of CD122/CD132 blockade on OT-I T cell expansion in tumours. **g-j**, Effect of anti-CD122 and anti-CD132 (anti-CD122/CD132) treatment on OT-I TIL expansion in WT mice with control or $Ptgs1/Ptgs2^{-/-}$ BRAF^{V600E}-OVA tumours or with MC38-OVA tumours, analysed 11 days after tumour transplantation. **g,h**, Flow cytometry plots (**g**) and OT-I TIL numbers (**h**) in BRAF^{V600E}-OVA tumours ($n = 6$). **i,j**, Flow cytometry plots (**i**) and OT-I TIL numbers (**j**) in MC38-OVA tumours ($n = 10$). **k**, Experimental design for **l** and **m** with MC38-OVA tumours. **l**, Flow cytometry plot (left) and quantification (right) of OT-I TILs at day 10 ($n = 6$). **m**, Flow

cytometry plots showing the population size of TIM-3⁺CXCR6⁺ cells among control and $Cd122^{-/-}$ $Cd4^{cre}Ptger2^{-/-}Ptger4^{fl/fl}$ OT-I TILs. **n**, WT mice received 1×10^3 naive OT-I T cells or 1×10^3 naive $Cd4^{cre}Ptger2^{-/-}Ptger4^{fl/fl}$ OT-I T cells intravenously (i.v.) and were transplanted s.c. with 2×10^6 MC38-OVA cells before analysis of tumour growth over time ($n = 10$). Asterisk indicates that termination criteria were reached. Data in **c, d, f, h, j, l** and **n** are pooled from two (**c, d, h, l**) or three (**f, j, n**) independent experiments and depicted as box plots extending from the 25th to 75th percentiles with the median as the centre and the whiskers corresponding to minimum and maximum values (**c, d, h, j, l**) or shown as the mean \pm s.e.m. (**f, n**). Plots in **b, e, g, i, l** and **m** show data for 1 sample representative of $n = 6$ samples analysed in 2 (**b, g, i, l**) or 3 (**e, i**) independent experiments. P values are from paired t -tests (**l**), one-way ANOVA with Tukey's multiple-comparison test (**c, d**) or Dunnett's multiple-comparison test (**h, j**), or two-way ANOVA with Bonferroni's correction for multiple testing (**n**).

initial phase of tumour infiltration (Fig. 4b,d), EP₂/EP₄-deficient OT-I T cells underwent persistent expansion in tumour tissue (Fig. 4b,d). Similarly, EP₂-deficient OT-I T cells showed inefficient intratumoural expansion compared with EP₂/EP₄-deficient OT-I T cells (Extended Data Fig. 9a,b). Notably, EP₂/EP₄-deficient TCF1⁺ OT-I TILs over time gave rise to phenotypically distinct populations of TIM-3⁺CXCR6⁺ effector cells (Extended Data Fig. 9c,d). Re-transfer experiments (Extended Data Fig. 9e,f) confirmed that EP₂/EP₄-deficient TIM-3⁺ (TCF1⁺) OT-I TILs but not their TIM-3⁺ (TCF1⁻) descendants possessed the capacity to

expand in tumours (Extended Data Fig. 9g,h) and were able to give rise to TIM-3⁺CXCR6⁺ TILs (Extended Data Fig. 9i). In separate experiments, we also observed that the development of TIM-3⁺ effector progeny from TCF1⁺ EP₂/EP₄-deficient OT-I T cells exclusively occurred in tumours but not in tdLNs (Fig. 4e,f and Extended Data Fig. 9j). Together, these data suggest that clonal T cell effector differentiation is restricted to tumour tissue and originates from TCF1⁺ TILs¹⁻³. Consistent with this notion, and similar to our observations for polyclonal anticancer CD8⁺ T cell responses, FTY720-mediated blockade of T cell egress

from LNs from day 6 onwards had no impact on the local expansion of EP₂/EP₄-deficient OT-I TILs (Extended Data Fig. 9k,l). We conclude that tumour-specific TCF1⁺ TILs expand and give rise to effector progeny within tumours, and this pivotal phase of the anticancer CD8⁺ T cell responses is blunted by PGE₂.

In vivo blockade of IL-2R signalling using blocking antibodies against the IL-2Rβ (also known as CD122) and IL-2Rγc (also known as CD132) chains abrogated the expansion advantage of OT-I TILs in PGE₂-deficient *Ptgs1/Ptgs2*^{-/-} BRAF^{V600E}-OVA tumours (Fig. 4g,h) and that of EP₂/EP₄-deficient OT-I TILs in PGE₂-producing MC38-OVA tumours (Fig. 4i,j). Similar results were observed after T cell-specific ablation of IL-2Rβ expression (Fig. 4k), which resulted in markedly reduced expansion (Fig. 4l) and effector differentiation (Fig. 4m) of EP₂/EP₄-deficient OT-I TILs compared with mock-treated control EP₂/EP₄-deficient OT-I TILs. Therefore, the IL-2R signalling pathway drives the expansion and effector differentiation of antigen-specific CD8⁺ TILs in the absence of PGE₂-EP₂/EP₄ signalling.

Finally, to specifically evaluate whether EP₂/EP₄-deficient antigen-specific CD8⁺ T cells mount protective anticancer responses, we analysed the growth of MC38-OVA tumours transplanted into WT mice with or without transfer of WT or EP₂/EP₄-deficient OT-I T cells. EP₂/EP₄-deficient OT-I T cells achieved complete rejection of MC38-OVA tumours, whereas WT OT-I T cells failed to affect progressive MC38-OVA tumour growth (Fig. 4n). Of note, EP₂/EP₄-deficient OT-I but not WT OT-I TILs also showed enhanced expansion that led to efficient tumour elimination in mouse melanoma D4M.3A-pOVA tumours (Extended Data Fig. 9m,n). Taken together, these results suggest that interfering with the PGE₂-EP₂/EP₄ axis in cancer-specific CD8⁺ T cells can elicit their expansion and effector differentiation within tumours and result in protective T cell-mediated anticancer immunity.

Discussion

Our results demonstrate that tumour-derived PGE₂ acts locally within the tumour microenvironment to limit CD8⁺ TIL expansion and effector differentiation originating from TCF1⁺ stem-like TILs. This inhibitory mechanism is crucial for cancer immune escape. We reveal that PGE₂-mediated restriction of TIL responses generated from TCF1⁺ TILs depends on TIL-intrinsic signalling of the PGE₂-receptors EP₂ and EP₄, which causes downregulation of functional IL-2 receptors and curtails TIL responsiveness to IL-2. As a result, interference with PGE₂-EP₂/EP₄ signalling in CD8⁺ T cells enhances their IL-2 responsiveness and induces protective TIL-mediated anticancer immunity. Of note, the effect of PGE₂ on TIL expansion and effector differentiation may at least in part be linked to a defect in IL-2-dependent mTORC1 signalling, as also suggested by an accompanying paper³⁷.

Beyond highlighting that clonal expansion and effector differentiation of stem-like TCF1⁺CD8⁺ T cells occurs within tumour tissue, as recently suggested¹⁻³, our results reveal that this critical phase of protective anticancer immunity is selectively targeted by tumour-derived PGE₂. These findings therefore identify an intratumoural checkpoint that locally controls expansion and effector differentiation of cancer-specific CD8⁺ TILs. Of note, this mechanism may act in parallel to PGE₂-mediated inhibition of cDC1 (ref. 38), which can support TCF1⁺ TIL responses within the tumour microenvironment³⁹.

Our unbiased transcriptional profiling by scRNA-seq uncovered that protective anticancer responses by EP₂/EP₄-deficient TILs are coupled to a rescue of IL-2 signalling. Recent studies have highlighted the relevance of IL-2 signalling for the generation of effective CD8⁺ T cell responses from antigen-specific TCF1⁺CD8⁺ T cells^{6,34,40,41}. Therefore, the discovery that the PGE₂-EP₂/EP₄ axis antagonizes the responsiveness of TCF1⁺ TILs to IL-2 has important mechanistic and clinical implications. Our results provide evidence that PGE₂ limits the proliferative capacity (and hence likely the self-renewal) of TCF1⁺ stem-like TILs and at the same time curbs effector T cell generation

along the entire pathway of intratumoural TIL differentiation. Importantly, ablation of PGE₂ signalling and consequently reconstitution of IL-2 signalling sufficed to achieve clonal TIL expansion and their effector differentiation within tumours that was not accompanied while preserving TCF1⁺ stem-like TILs. This is fundamentally different to interfering with exhaustion-inducing transcription factors such as TOX or MYB, which comes at the expense of TCF1⁺ stem-like CD8⁺ T cells and leads to a substantial change towards the development of terminally differentiated dysfunctional T cells²⁶⁻²⁸. Moreover, our finding that abrogating PGE₂ signalling in T cells enhances clonal expansion across the entire differentiation spectrum of anticancer TILs indicates that physiological IL-2 concentrations within tumours are sufficient to drive protective anticancer immunity if IL-2 signalling in TILs is restored.

Targeting EP₂ and EP₄ on anticancer T cells to overcome PGE₂-induced curtailing of IL-2 responsiveness might be preferential over using high concentrations of IL-2, as the latter may lead to deleterious off-target effects of IL-2 on IL-2R-expressing lung endothelial cells or CD4⁺ regulatory T cells⁴². On this note, ablation of the PGE₂-EP₂/EP₄ signalling axis to enhance IL-2 responsiveness in adoptively transferred cancer-specific CD8⁺ T cells bears the promise to unleash their full potential to mount protective anticancer immunity not only in mice but also in cancer patient-derived TILs, as demonstrated in the accompanying paper³⁷. Given the association of increased COX-mediated PGE₂ production in tumours with cancer growth and poor survival rates in patients with cancer, our findings therefore identify the PGE₂-EP₂/EP₄ signalling axis in TILs as molecular target to improve T cell immune therapy in cancer patients with PGE₂-producing tumours. This strategy may further be beneficial in tumours that produce high levels of other EP₂/EP₄-engaging prostanoids such as PGF_{2α}, PGD₂ and PGI₂ (ref. 43).

Online content

Any methods, additional references, Nature Portfolio reporting summaries, source data, extended data, supplementary information, acknowledgements, peer review information; details of author contributions and competing interests; and statements of data and code availability are available at <https://doi.org/10.1038/s41586-024-07254-x>.

- Jansen, C. S. et al. An intra-tumoral niche maintains and differentiates stem-like CD8 T cells. *Nature* **576**, 465–470 (2019).
- Siddiqui, I. et al. Intratumoral Tcf1⁺PD-1⁺ CD8⁺ T cells with stem-like properties promote tumor control in response to vaccination and checkpoint blockade immunotherapy. *Immunity* **50**, 195–211.e10 (2019).
- Prokhnevska, N. et al. CD8⁺ T cell activation in cancer comprises an initial activation phase in lymph nodes followed by effector differentiation within the tumor. *Immunity* **56**, 107–124.e5 (2023).
- Zehn, D., Thimme, R., Lugli, E., de Almeida, G. P. & Oxenius, A. ‘Stem-like’ precursors are the fount to sustain persistent CD8⁺ T cell responses. *Nat. Immunol.* **23**, 836–847 (2022).
- Miller, B. C. et al. Subsets of exhausted CD8⁺ T cells differentially mediate tumor control and respond to checkpoint blockade. *Nat. Immunol.* **20**, 326–336 (2019).
- Codarri Deak, L. et al. PD-1-cis IL-2R agonism yields better effectors from stem-like CD8⁺ T cells. *Nature* **610**, 161–172 (2022).
- Krishna, S. et al. Stem-like CD8 T cells mediate response of adoptive cell immunotherapy against human cancer. *Science* **370**, 1328–1334 (2020).
- Liu, B. et al. Temporal single-cell tracing reveals clonal revival and expansion of precursor exhausted T cells during anti-PD-1 therapy in lung cancer. *Nat. Cancer* **3**, 108–121 (2022).
- Kurtulus, S. et al. Checkpoint blockade immunotherapy induces dynamic changes in PD-1-CD8⁺ tumor-infiltrating T cells. *Immunity* **50**, 181–194.e6 (2019).
- Gatto, F., Schulze, A. & Nielsen, J. Systematic analysis reveals that cancer mutations converge on deregulated metabolism of arachidonate and xenobiotics. *Cell Rep.* **16**, 878–895 (2016).
- Wang, D. & DuBois, R. N. Eicosanoids and cancer. *Nat. Rev. Cancer* **10**, 181–193 (2010).
- Wang, Q., Morris, R. J., Bode, A. M. & Zhang, T. Prostaglandin pathways: opportunities for cancer prevention and therapy. *Cancer Res.* **82**, 949–965 (2022).
- Finetti, F. et al. Prostaglandin E2 and cancer: insight into tumor progression and immunity. *Biology* **9**, 434 (2020).
- Zelenay, S. et al. Cyclooxygenase-dependent tumor growth through evasion of immunity. *Cell* **162**, 1257–1270 (2015).
- Böttcher, J. P. et al. NK cells stimulate recruitment of cDC1 into the tumor microenvironment promoting cancer immune control. *Cell* **172**, 1022–1037.e14 (2018).
- Kalinski, P. Regulation of immune responses by prostaglandin E2. *J. Immunol.* **188**, 21–28 (2012).

17. Chen, J. H. et al. Prostaglandin E2 and programmed cell death 1 signaling coordinately impair CTL function and survival during chronic viral infection. *Nat. Med.* **21**, 327–334 (2015).
18. Mosenden, R. et al. Mice with disrupted type I protein kinase A anchoring in T cells resist retrovirus-induced immunodeficiency. *J. Immunol.* **186**, 5119–5130 (2011).
19. Newick, K. et al. Augmentation of CAR T-cell trafficking and antitumor efficacy by blocking protein kinase A localization. *Cancer Immunol. Res.* **4**, 541–551 (2015).
20. Lone, A. M. & Taskén, K. Phosphoproteomics-based characterization of prostaglandin E2 signaling in T cells. *Mol. Pharmacol.* **99**, 370–382 (2021).
21. Roberts, E. W. et al. Critical role for CD103⁺/CD141⁺ dendritic cells bearing CCR7 for tumor antigen trafficking and priming of T cell immunity in melanoma. *Cancer Cell* **30**, 324–336 (2016).
22. Spranger, S., Bao, R. & Gajewski, T. F. Melanoma-intrinsic β -catenin signalling prevents anti-tumour immunity. *Nature* **523**, 231–235 (2015).
23. Böttcher, J. P. et al. Functional classification of memory CD8⁺ T cells by CX3CR1 expression. *Nat Commun.* **6**, 8306 (2015).
24. Zander, R. et al. CD4⁺ T cell help is required for the formation of a cytolytic CD8⁺ T cell subset that protects against chronic infection and cancer. *Immunity* **51**, 1028–1042.e4 (2019).
25. Aandahl, E. M. et al. CD7 is a differentiation marker that identifies multiple CD8 T cell effector subsets. *J. Immunol.* **170**, 2349–2355 (2003).
26. Alfei, F. et al. TOX reinforces the phenotype and longevity of exhausted T cells in chronic viral infection. *Nature* **571**, 265–269 (2019).
27. Scott, A. C. et al. TOX is a critical regulator of tumour-specific T cell differentiation. *Nature* **571**, 270–274 (2019).
28. Tsui, C. et al. MYB orchestrates T cell exhaustion and response to checkpoint inhibition. *Nature* **609**, 354–360 (2022).
29. Yost, K. E. et al. Clonal replacement of tumor-specific T cells following PD-1 blockade. *Nat. Med.* **25**, 1251–1259 (2019).
30. Lucca, L. E. et al. Circulating clonally expanded T cells reflect functions of tumor-infiltrating T cells. *J. Exp. Med.* **218**, e20200921 (2021).
31. Mandala, S. et al. Alteration of lymphocyte trafficking by sphingosine-1-phosphate receptor agonists. *Science* **296**, 346–349 (2002).
32. Ross, S. H. & Cantrell, D. A. Signaling and function of interleukin-2 in T lymphocytes. *Annu. Rev. Immunol.* **36**, 411–433 (2018).
33. Hashimoto, M. et al. PD-1 combination therapy with IL-2 modifies CD8⁺ T cell exhaustion program. *Nature* **610**, 173–181 (2022).
34. Corria-Osorio, J. et al. Orthogonal cytokine engineering enables novel synthetic effector states escaping canonical exhaustion in tumor-rejecting CD8⁺ T cells. *Nat. Immunol.* **24**, 869–883 (2023).
35. Di Pilato, M. et al. CXCR6 positions cytotoxic T cells to receive critical survival signals in the tumor microenvironment. *Cell* **184**, 4512–4530.e22 (2021).
36. Danilo, M., Chennupati, V., Silva, J. G., Siebert, S. & Held, W. Suppression of Tcf1 by inflammatory cytokines facilitates effector CD8 T cell differentiation. *Cell Rep.* **22**, 2107–2117 (2018).
37. Morotti, M. et al. PGE₂ inhibits TIL expansion by disrupting IL-2 signalling and mitochondrial function. *Nature* <https://doi.org/10.1038/s41586-024-07352-w> (2024).
38. Bayerl, F. et al. Tumor-derived prostaglandin E2 programs cDC1 dysfunction to impair intratumoral orchestration of anti-cancer T cell responses. *Immunity* **56**, 1341–1358.e11 (2023).
39. Meiser, P. et al. A distinct stimulatory cDC1 subpopulation amplifies CD8⁺ T cell responses in tumors for protective anti-cancer immunity. *Cancer Cell* **41**, 1498–1515.e10 (2023).
40. Mo, F. et al. An engineered IL-2 partial agonist promotes CD8⁺ T cell stemness. *Nature* **597**, 544–548 (2021).
41. Tichet, M. et al. Bispecific PD1-IL2v and anti-PD-L1 break tumor immunity resistance by enhancing stem-like tumor-reactive CD8⁺ T cells and reprogramming macrophages. *Immunity* **56**, 162–179.e6 (2023).
42. Leonard, W. J., Lin, J.-X. & O’Shea, J. J. The yc family of cytokines: basic biology to therapeutic ramifications. *Immunity* **50**, 832–850 (2019).
43. Biringir, R. G. A review of prostanoid receptors: expression, characterization, regulation, and mechanism of action. *J. Cell Commun. Signal.* **15**, 155–184 (2021).

Publisher’s note Springer Nature remains neutral with regard to jurisdictional claims in published maps and institutional affiliations.



Open Access This article is licensed under a Creative Commons Attribution 4.0 International License, which permits use, sharing, adaptation, distribution and reproduction in any medium or format, as long as you give appropriate credit to the original author(s) and the source, provide a link to the Creative Commons licence, and indicate if changes were made. The images or other third party material in this article are included in the article’s Creative Commons licence, unless indicated otherwise in a credit line to the material. If material is not included in the article’s Creative Commons licence and your intended use is not permitted by statutory regulation or exceeds the permitted use, you will need to obtain permission directly from the copyright holder. To view a copy of this licence, visit <http://creativecommons.org/licenses/by/4.0/>.

© The Author(s) 2024

Methods

Mice

All mice used in this study were on a C57BL/6J genetic background and purchased from the Jackson Laboratory (JAX). OT-I × CD45.1 mice were generated by crossing OT-I mice (JAX, 003831) to CD45.1 (JAX, 002014) mice. *Ptger2*^{-/-}*Ptger4*^{fl/fl} mice were generated by crossing *Ptger2*^{-/-} mice (JAX, 004376) to *Ptger4*^{fl/fl} mice (JAX, 028102) and further crossed to *Cd4*^{cre} mice (JAX, 022071) to generate *Cd4*^{cre}*Ptger2*^{-/-}*Ptger4*^{fl/fl} mice or crossed to *Gzmb*^{cre} mice (JAX, 003734) to generate *Gzmb*^{cre}*Ptger2*^{-/-}*Ptger4*^{fl/fl} mice. Unless stated otherwise, mice were on a CD45.2/CD45.2 background. For some experiments, *Cd4*^{cre}*Ptger2*^{-/-}*Ptger4*^{fl/fl} mice and *Ptger2*^{-/-}*Ptger4*^{fl/fl} mice were crossed to OT-I mice to generate *Cd4*^{cre}*Ptger2*^{-/-}*Ptger4*^{fl/fl} OT-I mice and *Ptger2*^{-/-}*Ptger4*^{fl/fl} OT-I mice and used on a CD45.1/CD45.2 or CD45.1/CD45.1 background. WT or *Rag1*^{-/-} mice (JAX, 002216) on a CD45.2/CD45.2 background were used as recipients in adoptive transfer experiments. In all experiments, mice at 6–12 weeks of age were sex-matched and randomly assigned to control or treatment groups. Mouse experiments with *Ptgs1/Ptgs2*^{-/-} BRAF^{V600E} tumours and T cell depletion were conducted without blinding; all other experiments were performed in a blinded manner. No statistical methods were used to predetermine sample sizes. Mice were killed by cervical dislocation under anaesthesia. All mice were maintained and bred at the Klinikum rechts der Isar, TUM, or at the Klinikum der Universität München, LMU, under specific-pathogen-free, controlled conditions with a 12-h light–dark cycle, ambient temperature of 24 °C and humidity maintained at 55%, and in accordance with the guidelines of the Federation of European Laboratory Animal Science Associations. All animal experiments were performed in accordance with the guidelines of the district government of upper Bavaria (Department 5–Environment, Health and Consumer Protection).

Cell lines

Control and *Ptgs1/Ptgs2*^{-/-} BRAF^{V600E} melanoma cells were generated using the CRISPR–Cas9 system as previously described¹⁴. BRAF^{V600E}-OVA and *Ptgs1/Ptgs2*^{-/-} BRAF^{V600E}-OVA cells were generated by lentiviral transduction. In brief, OVA cDNA was subcloned into a pHIV-7 transfer vector carrying both the phosphoglycerate kinase (*PGK*) promoter and IRES-puromycin-resistance sequence. The production of third-generation self-inactivating lentiviral vectors, pseudotyped with VSV-G, was carried out as previously described⁴⁴. Specifically, packaging cells were transfected and, after 2 days, cell supernatants were collected, filtered and used to transduce tumour cell lines in the presence of 8 µg ml⁻¹ polybrene (Merck). After the incubation period, medium was exchanged for fresh medium, and target cells were passaged at least three times after transduction and selected using puromycin. MC38 cells were provided by A. Krüger, Institute of Experimental Oncology, TUM, and MC38-OVA and Panc02 cells were provided by V. Buchholz, Institute for Medical Microbiology, Immunology and Hygiene, TUM.

BRAF^{V600E}, *Ptgs1/Ptgs2*^{-/-} BRAF^{V600E}, BRAF^{V600E}-OVA and *Ptgs1/Ptgs2*^{-/-} BRAF^{V600E}-OVA cells were cultured in complete RPMI medium (RPMI 1640 medium (Thermo Fisher Scientific) supplemented with 10% FCS (Merck), 50 µM β-mercaptoethanol (Thermo Fisher Scientific), 50 U ml⁻¹ penicillin (Thermo Fisher Scientific), 50 µg ml⁻¹ streptomycin (Thermo Fisher Scientific) and 2 mM L-glutamine (Thermo Fisher Scientific). D4M.3A-pOVA cells were generated as previously described⁴⁵ and cultured in DMEM-F12 medium (Thermo Fisher Scientific). MC38, MC38-OVA and Panc02 cells were cultured in DMEM (Thermo Fisher Scientific), with both media supplemented with 10% FCS, 50 µM β-mercaptoethanol, 50 U ml⁻¹ penicillin, 50 mg ml⁻¹ streptomycin, 2 mM L-glutamine, 1 × MEM non-essential amino acids solution (Thermo Fisher Scientific) and 1 mM sodium pyruvate (Thermo Fisher Scientific). To generate tumour cell conditioned medium (CM), 5 × 10⁶ tumour cells were cultured in 20 ml complete RPMI medium for 48 h and the

supernatant was collected, filtered and stored at –20 °C until further use. All cell lines were routinely tested for mycoplasma contamination in-house by PCR. For *Ptgs1/Ptgs2*^{-/-} BRAF^{V600E} cells, the absence of PGE₂ production was routinely confirmed by PGE₂ ELISA (Cayman Chemical). No further cell line authentications were conducted in the laboratory.

Tumour cell injections

Tumour cell lines were detached by trypsinization (Thermo Fisher Scientific) and washed three times in sterile PBS (Thermo Fisher Scientific). Unless stated otherwise, 2 × 10⁶ cells were injected s.c. in 100 µl sterile PBS into the flank of each recipient mouse. Tumour growth was measured using a digital calliper. Tumour diameters stated in the figures refer to the average values of the longest diameter and its perpendicular for each tumour. A maximal tumour diameter of 15 mm served as the humane end point and was not exceeded in any of the experiments.

CD4⁺ and CD8⁺ T cell depletion in vivo

To deplete CD4⁺ and CD8⁺ T cells, mice received intraperitoneal (i.p.) injections of 100 µl anti-mouse CD4 (100 µg per mouse, GK1.5, BioXCell) or anti-mouse CD8β (100 µg per mouse, 53-5.8, BioXCell) antibodies every 5 days, beginning on day 1 following tumour cell inoculation.

FTY720 treatment in vivo

FTY720 treatment was performed by injecting mice i.p. with 100 µl of FTY720 (20 µg per mouse, Merck) on day 1 or day 6 after tumour cell transplantation. Injection with 100 µl sterile isotonic NaCl served as control.

IL-2 receptor blockade in vivo

For blockade of IL-2Rβ and IL-2Rγc, mice received i.p. injections of 150 µl anti-mouse CD122 (300 µg per mouse, TM-Beta1, BioXCell) and anti-mouse CD132 (300 µg per mouse, 3E12, BioXCell) antibodies on days 6 and 7 after tumour cell transplantation. Injections with 150 µl sterile isotonic NaCl served as control.

Processing of tumour tissue and lymphoid organs

Tumours, tLNs or spleens of tumour-bearing mice were excised at the indicated time points after cell transplantation. Tumour or organ weight was determined using a microscale. For subsequent analyses by flow cytometry or cell sorting, tumour samples were mechanically dissociated and incubated with collagenase IV (200 U ml⁻¹, Thermo Fisher Scientific) and DNase I (100 µg ml⁻¹, Merck) for 40 min at 37 °C and filtered through a 70 µm and a 30 µm cell strainer (Miltenyi) to generate single-cell suspensions. Spleens were passed through a 70 µm cell strainer, followed by red blood cell lysis and a second filtration step using a 30 µm cell strainer. LNs were passed through a 30 µm cell strainer. For the isolation of migratory cDC1s, LNs were processed as described for tumour samples.

Antibodies and reagents for flow cytometry and cell sorting

The following antibodies and staining reagents were used for flow cytometry or cell sorting: fixable viability dye eFluor 450 (dilution: 1:500; Thermo Fisher Scientific); fixable viability dye APC-eF780 (1:1,000; Thermo Fisher Scientific); viability dye SYTOX-blue (1:2,000; Thermo Fisher Scientific); APC anti-CD3 (1:100; clone 17A2, Thermo Fisher Scientific); PE anti-CD4 (1:200; GK1.5, Biolegend); AF647 anti-CD4 (1:200; GK1.5, Biolegend); PerCP/Cy5.5 anti-CD4 (1:200; GK1.5, Biolegend); BV421 anti-CD8α (1:200; 53-6.7, Biolegend); FITC anti-CD8α (1:200; 53-6.7, Biolegend); PE-Dazzle594 anti-CD8α (1:200; 53-6.7, Biolegend); PE-Cy7 anti-CD8α (1:200; 53-6.7, Biolegend); BV605 anti-CD11b (1:200; MI/70, Biolegend); PE-Cy7 anti-CD11c (1:200; N418, Biolegend); BV570 anti-mouse/human-CD44 (1:100; IM7, Biolegend); BV711 anti-mouse/human-CD44 (1:100; IM7, Biolegend); FITC anti-mouse/human-CD44 (1:100; IM7, Biolegend); PerCP-Cy5.5 anti-mouse/

human-CD44 (1:100; IM7, Biolegend); AF647 anti-CD45.1 (1:100; A20, Biolegend); PE anti-CD45.1 (1:100; A20, Biolegend); PE-Dazzle594 anti-CD45.1 (1:100; A20, Biolegend); PerCP/Cy5.5 anti-CD45.1 (1:100; A20, Biolegend); BV510 anti-CD45.2 (1:100; 104, Biolegend); FITC anti-CD45.2 (1:100; 104, Biolegend); PerCP-Cy5.5 anti-CD45.2 (1:100; 104, Biolegend); FITC anti-CD62L (1:100; MEL-14, Biolegend); PE-Dazzle594 anti-CD62L (1:100; MEL-14, Biolegend); FITC anti-CD103 (1:100; M290, BD Biosciences); APC anti-CD132/IL2R γ (1:100; TUGm2, Biolegend); PE-Dazzle594 anti-CD186/CXCR6 (1:200; SA051D1, Biolegend); PE anti-CX₃CR1 (1:100; SA011F11, Biolegend); BV605 anti-CD279/PD-1 (1:100; 29 F.1A12, Biolegend); BV421 anti-CD366/TIM-3 (1:200; RMT3-23, Biolegend); PerCP/Cy5.5 anti-TCR β (1:100; H57-597, Biolegend); AF700 anti-I-A/I-E (1:500; MHC class II) (M5/114.15.2, Biolegend); PE anti-H-2K^b bound to SIINFEKL (1:100; 25-D1.16, Biolegend); APC anti-human GZMB (1:200; GB12, Thermo Fisher Scientific); FITC anti-Ki-67 (1:100; SolA-15, Thermo Fisher Scientific); AF700 anti-Ki-67 (1:100; SolA-15, Thermo Fisher Scientific); PE anti-TCF1/TCF7 (1:40; S33-966, BD Biosciences); AF488 anti-human pSTAT5 (0.03 μ g per test, 47/Stat5(pY694); BD Biosciences); eF660 anti-TOX (1:100; TXRX10, Thermo Fisher Scientific); eFluor660 Rat-IgG2a- κ isotype-control (1:100; eBR2a, Thermo Fisher Scientific); APC mouse-IgG1k isotype-control (1:200; P3.6.2.8.1, Thermo Fisher Scientific); AF488 mouse-IgG1k isotype-control (0.03 μ g per test; MOPC-21, Biolegend); and rabbit-anti-mouse-TCF1/TCF7 (1:100; C.725.7, Thermo Fisher Scientific). These were followed by AF647 donkey-anti-rabbit IgG (1:200; Poly4064, Biolegend) or DL488 donkey-anti-rabbit IgG (1:200; Poly4064, Biolegend). Unless stated otherwise, all antibodies were anti-mouse antibodies.

Flow cytometry and cell sorting

For staining of surface markers and viability dyes, cells were stained for 15 min at 4 °C in FACS buffer (PBS with 1% FCS and 2 mM EDTA). Staining of SIINFEKL–MHC class I complexes on cDC1s for analysis of OVA cross-presentation was performed for 40 min. For intracellular staining of GZMB, TCF1, Ki-67 and TOX, cells were fixed and permeabilized using the True-Nuclear Transcription Factor Buffer Set (Biolegend) according to the manufacturer's protocol. Intracellular staining was performed overnight in permeabilization buffer at 4 °C. For intracellular staining of pSTAT5, cells were fixed and permeabilized using BD Cytotfix (BD Biosciences) and BD Phosflow Perm Buffer III (BD Biosciences) according to the manufacturer's instructions (protocols II and III, BD Biosciences). For the detection of EdU incorporation, EdU was added to the culture at a final concentration of 15 μ M for the last 3 h of the experiment, and analysis was performed using an EdU Proliferation kit (iFluor 488, Abcam) according to the manufacturer's protocol.

Flow cytometry analyses were performed using a LSR Fortessa Cell Analyzer (BD Biosciences, BD FACSDiva software v.8.0.1 and v.9.0.1), a SP6800 Spectral Cell Analyzer (Sony Biotechnologies, spectral analyser software v.2.0.2.14140) or a SA3800 Spectral Cell Analyzer (Sony Biotechnologies, spectral analyser software v.2.0.5.54250). For flow cytometric quantification of cell numbers, CountBright Absolute Counting Beads (Thermo Fisher Scientific) were added to samples before analyses. For some experiments, CD8⁺ TILs (live CD45⁺CD3⁺CD8⁺ cells), stem-like *Cd4^{cre}Ptger2^{-/-}Ptger4^{fl/fl}* OT-I TILs (live CD45.1⁺CD8⁺CD44⁺TIM-3⁻CXCR6⁻) or differentiated effector *Cd4^{cre}Ptger2^{-/-}Ptger4^{fl/fl}* OT-I TILs (live CD45.1⁺CD8⁺CD44⁺TIM-3⁺CXCR6⁺) were sorted using a FACS Aria III Cell Sorter (BD Biosciences, BD FACSDiva software v.9.0.1). Naive OT-I T cells (CD45.1⁺CD8⁺CD62L⁺CD44⁻) used in adoptive transfer experiments were sorted from blood using a SH800S Cell Sorter (Sony Biotechnologies, cell sorter software v.2.1.6). All flow cytometric data were analysed using FlowJo (BD Biosciences, v.00.8.1 and v.10.8.2).

Adoptive T cell transfer

For adoptive T cell transfer of naive T cells, 1×10^3 congenically marked naive CD8⁺ T cells from OT-I, *Ptger2^{-/-}Ptger4^{fl/fl}* OT-I or

Cd4^{cre}Ptger2^{-/-}Ptger4^{fl/fl} OT-I donor mice were injected i.v. in sterile PBS into sex-matched recipient WT mice 6 h before tumour cell transplantation s.c. For adoptive transfer of CRISPR-Cas9-edited T cells, 1×10^3 cells congenically marked OT-I T cells from in vitro T cell cultures were injected i.v. into recipient mice at day 2 after tumour cell transplantation s.c. For re-transfer of CD8⁺ TILs, 7×10^3 congenically marked stem-like (TIM-3⁻CXCR6⁻) or differentiated effector (TIM-3⁺CXCR6⁺) *Cd4^{cre}Ptger2^{-/-}Ptger4^{fl/fl}* OT-I TILs were sorted from MC38-OVA tumours from WT mice and injected i.v. in sterile PBS into sex-matched recipient *Rag1^{-/-}* mice inoculated with MC38-OVA tumour cells 2 days before T cell re-transfer.

Generation of repetitively activated antigen-experienced TCF1⁺CD8⁺ T cells

TCF1⁺CD8⁺ T cells were differentiated from splenic naive CD8⁺ T cells by repetitive activation as previously described³⁵, with minor modifications. In brief, 1×10^6 naive CD8⁺ T cells were seeded in complete RPMI medium supplemented with $1 \times$ MEM non-essential amino acids solution and 1 mM sodium pyruvate. Low-dose IL-2 (85 U ml⁻¹) and mouse anti-CD3/CD28 microbeads were added to the culture while maintaining a CD8⁺ T cell concentration of 1×10^6 cells per ml for multiple (re-) activation cycles over a course of 4 days, followed by purification of live cells by gradient centrifugation (Pancoll).

T cell effector differentiation

Effector differentiation of TCF1⁺CD8⁺ T cells was performed as previously described³⁵, with minor modifications. In brief, cells were cultured with mouse anti-CD3/CD28 microbeads in the presence of high-dose IL-2 (350 U ml⁻¹). Where indicated, PGE₂ (100 ng ml⁻¹, unless indicated otherwise in the figure legend; Thermo Fisher Scientific), tumour cell CM, IL-7 (10 ng ml⁻¹, Miltenyi), IL-12 (10 ng ml⁻¹, Biolegend) or IL-15/15R α (1 ng ml⁻¹, Thermo Fisher Scientific) was added to the culture. To assess T cell expansion, the numbers of live CD45⁺CD3⁺CD8⁺ T cells were quantified by flow cytometry 72 h after the incubation period.

Gene deletion by CRISPR–Cas9–gRNA complex electroporation

Cd4^{cre}Ptger2^{-/-}Ptger4^{fl/fl} OT-I T cells were purified from spleen and cultured in complete RPMI supplemented with IL-2 (10 U ml⁻¹) and IL-7 (5 ng ml⁻¹) in the presence of mouse anti-CD3/CD28 microbeads. After 24 h, anti-CD3/CD28 microbeads were removed by magnetic separation and cells were electroporated (4D-Nucleofector, Lonza; pulse program CM137)⁴⁶ in P3 electroporation buffer supplemented with the Cas9 electroporation enhancer (IDT), Cas9 protein (IDT) and *Cd122*-targeting or non-targeting gRNAs. gRNAs were generated by hybridizing trRNA (IDT) with *Cd122*-targeting (sequences TATGTC AAGGAGGTC CA CCG and CTGGGAACGACCCGAGGATC, generated using CHOPCHOP; ref. 47) or non-targeting crRNA (IDT) (GCCTGCCCTAAACCCGGAA; ref. 48) as mock control. Cells were rested in complete RPMI supplemented with IL-7 (5 ng ml⁻¹, Miltenyi) at 37 °C for 48 h and validated for specific knockout by CD122 surface staining before injection into recipient mice.

Analysis of IL-2R γ expression and IL-2 signalling

TCF1⁺CD8⁺ T cells from in vitro cultures were rested for 20 h in complete RPMI supplemented with low-dose IL-2 and purified by gradient centrifugation. Cells were stimulated with mouse anti-CD3/CD28 microbeads and low-dose IL-2 for 24 h in the absence or presence of PGE₂ (100 ng ml⁻¹). After 24 h, IL-2R γ chain expression was analysed by flow cytometry. For analysis of IL-2-induced STAT5 signalling, anti-CD3/CD28 microbeads were removed by magnetic separation, cells were rested for 30 min at 37 °C in complete RPMI and stimulated for 30 min with different concentrations of IL-2 (10–100 U ml⁻¹, as indicated). After the incubation period, fixation buffer was directly added to the culture to terminate the signalling process and cells were stained for flow cytometry analysis.

PGE₂ measurements

Tumours and organs of tumour-bearing mice were excised 11 days after tumour cell transplantation, directly frozen in liquid nitrogen and stored at -80°C until further processing. Samples were homogenized in homogenization buffer (0.1 MPBS, 1 mM EDTA and 10 μM indomethacin (Merck), pH 7.4) using a gentleMACS Dissociator (Miltenyi) followed by a freeze–thaw cycle. PGE₂ concentrations were measured by ELISA (Cayman Chemical) according to the manufacturer's protocol.

RNA isolation and quantitative real-time PCR

RNA was isolated using an Arcturus PicoPure RNA isolation kit (Thermo Fisher Scientific) and cDNA was generated using a SensiFAST cDNA synthesis kit (Bioline). Quantitative real-time PCR was carried out on a LightCycler 480 (Roche, LightCycler 480 software v.1.5.1) using a TAKYON No ROX SYBR MasterMix dTTP Blue kit (Eurogentec) according to the manufacturer's protocol. *Ptger4* expression was determined using the ΔCt method, with *Hprt* serving as reference gene. Primer sequences were from a previous study³⁸. All primers were purchased from Eurofins.

scRNA-seq and scTCR-seq

CD8⁺ TILs were sorted from BRAF^{V600E} tumours 11 days after tumour cell transplantation. A combination of cell hashing and DNA barcoding during library preparation was used for sample multiplexing, which enabled the simultaneous sequencing of four biological replicates from each group. For cell hashing, unique TotalSeq-C anti-mouse hashtag antibodies were used for hashing of cells from each experimental group as follows: WT: hashtag 1; *Ptger2*^{-/-}*Ptger4*^{fl/fl}: hashtag 2; *Cd4*^{cre}*Ptger2*^{-/-}*Ptger4*^{fl/fl}: hashtag 3; and *Gzmb*^{cre}*Ptger2*^{-/-}*Ptger4*^{fl/fl}: hashtag 4 (1:250 each, Biolegend). Hashtagged cells from one tumour-bearing mouse of each group were pooled and loaded on a Chromium Next GEM Chip (10x Genomics). RNA-seq libraries were generated using Chromium Next GEM Single Cell 5' Reagent kits v.2 User Guide with Feature Barcode technology for Cell Surface Protein (Rev D) according to the manufacturer's protocol (10x Genomics). Quality control was carried out using a High Sensitivity DNA kit (Agilent), a Bioanalyzer 2100 and a Qubit dsDNA HS Assay kit (Thermo Fisher Scientific). For sequencing, libraries were pooled and analysed by paired-end sequencing (2 × 150 bp) on a NovaSeq6000 platform using S4 v.1.5 (300 cycles) sequencing kits (Illumina). Libraries were sequenced to a depth of at least 2 × 10⁴ reads per cell for gene expression libraries and 5 × 10³ reads per cell for T cell receptor libraries.

Initial scRNA-seq analyses were performed for all samples from the groups *Ptger2*^{-/-}*Ptger4*^{fl/fl}, *Cd4*^{cre}*Ptger2*^{-/-}*Ptger4*^{fl/fl} and *Gzmb*^{cre}*Ptger2*^{-/-}*Ptger4*^{fl/fl}, with data from the WT group being added at a later stage for validation of *Ptger2* and *Ptger4* read coverage (see below). Alignment of gene expression libraries and demultiplexing were performed using cellranger multi (Cell Ranger (v.6.1.1)⁴⁹; 10x Genomics) against the pre-built mouse reference v2020-A (10x Genomics, mm10/GRCm38, annotation from GENCODE Release M23) with the number of expected cells equals 21,000 as input argument. The BAM files were converted to FASTQ files using the tool bamtofastq with the argument --reads-per-fastq set to the total number of reads in the BAM file plus 10,000. After that, gene expression and TCR analysis were combined by running cellranger multi separately for each demultiplexed sample, disabling library concordance reinforcement. The algorithm was forced to find the number of cells identified in the first step of demultiplexing, and sample-specific FASTQ files were used as input for the gene expression analysis pipeline. The pre-built Ensembl GRCm38 Mouse V(D)J Reference v.5.0.0 was used for TCR analysis.

The initial downstream analysis was performed in R (v.4.0.4) with the R package Seurat (v.4.0.1)⁵⁰. Only cells with more than 1,000 genes detected, less than 10% of mitochondrial genes and with UMI counts

less than 3 standard deviations above the mean were kept. The data were filtered for genes detected in at least three cells in one of the samples. Filtered read counts from each sample were normalized independently using sctransform (v.0.3.2)⁵¹ with the glmGamPoi method⁵². Anchors between cells from different replicates were identified on the top 1,000 highly variable genes using canonical correlation analysis and 30 canonical vectors. Data integration was performed on first 20 PC analysis (PCA) dimensions. PCA was calculated for the integrated data on the top 1,000 highly variable genes and both *k*-nearest neighbour graph and UMAP were computed on the 30 nearest neighbours and first 20 PCA dimensions. Louvain clusters were identified using the shared nearest neighbour modularity optimization-based algorithm at resolutions 0.9, 0.65 and 0.9 for the groups *Ptger2*^{-/-}*Ptger4*^{fl/fl}, *Cd4*^{cre}*Ptger2*^{-/-}*Ptger4*^{fl/fl} and *Gzmb*^{cre}*Ptger2*^{-/-}*Ptger4*^{fl/fl}, respectively. Contaminating myeloid cells were identified based on the average cluster expression of the marker genes *Cd14*, *Ly2z*, *Fcgr3*, *Ms4a7*, *Fcer1g*, *Cst3*, *H2-Aa*, *Ly6d*, *Ms4a1* and *Ly6d*. Cycling cells were identified based on expression of *Cdk1*, *Mcm2*, *Pclaf*, *H2afz*, *Birc5* and *Mki67*.

The integrative analysis between groups was performed in R (v.4.2.1) with the R package Seurat (v.4.1.1)⁵⁰. After general data pre-processing and regression of contaminating cells as mentioned above, filtered read counts from each sample were normalized independently using sctransform (v.0.3.2)⁵¹ with glmGamPoi method⁵². Anchors between cells from all groups and all their replicates were identified using a more conservative approach, which led to weaker batch correction. For that purpose, reciprocal PCA was applied on the top 1,000 highly variable genes of each sample and anchors were picked using the first 20 dimensions and 1 neighbour only. PCA was performed on the integrated data on the top 1,000 highly variable genes. A *k*-nearest neighbour graph and UMAP (spread of 0.4, minimum distance of 0.01) were computed on the first 20 PCs and 30 nearest neighbours. A resolution of 0.6 was used for Louvain clusters identification using the shared nearest neighbour modularity optimization-based algorithm. DEGs between two groups were identified using the Wilcoxon rank-sum test and Bonferroni correction. Gene set expression scores at single-cell level were calculated using the AddModuleScore function, including only the detected genes. Similarity scores with reference datasets were calculated using the R package SingleR (v.1.10.0)⁵³ with the top 200 DEGs. The processed transcriptome profiles of naive CD8⁺ T cells, memory stem cell CD8⁺ T cells and central memory CD8⁺ T cells were from a previous study⁵⁴. For tumour antigen-specific CD8⁺ T cells in tdLNs, tumour-infiltrating stem-like CD8⁺ T cells and their naive counterparts, data from a previous study³ were processed using the R package DESeq2 (v.1.36)⁵⁵. Gene set expression scores at the single-cell level were calculated using the AddModuleScore function, including only the detected genes. The effector T cell gene signature was from a previous study⁵⁶ (M3013: KAECH_NAIVE_VS_DAY8_EFF_CD8_TCELL_DN). The CD8⁺ T cell proliferation signature was obtained from MSigDB (GO:2000566). Transcriptional trajectories were inferred using the R package slingshot (v.2.4.0)⁵⁷ over the UMAP calculated on the integrated data, approximating the curves by 150 points. The pseudotime was calculated as a weighted average across lineages, weighted by the assignment weight.

TCR analysis of clonotype was performed using the R package scRepertoire (v.1.6.0)⁵⁸. Clonotypes were called based on a combination of VDJC genes comprising the TCR and the nucleotide sequence of the CDR3 region. Whenever the clonotype distribution is shown for individual groups, the cell number was downsampled, so that cluster 1 from all groups had the same maximum size. TF activity was inferred using the weighted mean method of decoupleR (v.2.2.2)⁵⁹ and TF–target interactions available through dorothea (v.1.8.0)⁶⁰, with confidence levels A to C. Normalization to *Ptger2*^{-/-}*Ptger4*^{fl/fl} was achieved by subtracting its scores from the scores of the other groups. The top 100 variable TFs between clusters within each group were

used to draw a network graph with tidygraph (v.1.2.1)⁶¹ based on common targets with same defined mode of regulation as defined on the database. Only TFs with at least two common targets were kept for visualization. Louvain clusters were identified using igraph (v.1.3.2)⁶² at a resolution of 0.5.

For addition of scRNA-seq data from the WT group, samples were pre-processed as described above and mapped to a reference formed by the integrated data of the *Ptger2*^{-/-}*Ptger4*^{fl/fl}, *Cd4*^{cre}*Ptger2*^{-/-}*Ptger4*^{fl/fl} and *Gzmb*^{cre}*Ptger2*^{-/-}*Ptger4*^{fl/fl} groups using the R package Seurat (v.4.1.1)⁵⁰. For that purpose, anchors between cells from the reference and the WT groups along with all replicates were identified using reciprocal PCA on top 1,000 highly variable genes. Anchors were picked using the first 20 dimensions and 1 neighbour only. Annotations were transferred using the function TransferData, and data were integrated using IntegrateEmbeddings. Cells from the added group were then projected onto the coordinates of the reference UMAP calling ProjectUMAP with 30 nearest neighbours. Read coverage was estimated using deepTools (v.3.5.4)⁶³ with bamCoverage and a bin size of 10 bp and normalization by bins per million mapped reads. For coverage analysis on *Tcf7*/TCF1⁺ and *Tcf7*/TCF1⁻ clusters, BAM files were split by cell barcodes from clusters 1–2 or clusters 3–8 using samtools (v.1.13)⁶⁴ before coverage estimation. Read coverage on gene tracks was visualized using the R package trackViewer (v.1.32.1)⁶⁵.

RNA-seq

In vitro generated, repetitively activated TCF1⁺CD8⁺ T cells were incubated in the presence or absence of PGE₂ (100 ng ml⁻¹) for 1 h at 37 °C followed by stimulation with IL-2 or IL-2 plus mouse anti-CD3/CD28 microbeads for an additional 4 h. Total RNA was isolated using Total RNA Miniprep (Monarch). Library preparation was carried out using a NEB Next UltraRNA Library Prep kit with i7 and i5 index reads of 8 bp each for mRNA library preparation and poly A enrichment. Sequencing was performed on a NovaSeq6000 PE150 platform in paired-end mode (read 1: 151 bp, read 2: 151 bp), using S4 (v.1.5) (300 cycles) sequencing kits (Illumina). Reads were aligned to the mouse reference genome (GRCm38/mm10, NCBI) using the Hisat2 (v.2.0.5) mapping tool. To quantify gene expression levels, featureCounts (v.1.5.0-p3) was used to count the reads mapped to each gene, followed by the calculation of fragments per kilobase of transcript sequence per million mapped reads based on gene length and read count. DEGs were identified using the DESeq2 R package (v.1.20.0). Adjusted *P* values were obtained using Wald test with multiple testing by the Benjamini–Hochberg method, and genes identified by DESeq2 with adjusted *P* values < 0.05 and fold change ≥ 2 were assigned as DEGs. Volcano plots were visualized using the ggplot2 R package ggplot2 (v.3.4.2), and PCA was conducted using the prcomp function in R and visualized using the R packages ggplot2 and ggrepel (v.0.9.3). DEGs obtained from comparing the groups ‘anti-CD3/CD28 +IL-2’ and ‘PGE₂-treated + anti-CD3/CD28 +IL-2’ were ordered based on their log₂ fold change values and subjected to GSEA using GSEA (v.4.3.2) probing for hallmark genes from mh.all.v2023.1.Mm (MSigDB). The PreRanked tool from GSEA (v.4.3.2) was used to determine the NES and significance by adjusted *P* values.

Statistical analyses

The GraphPad Prism software (v.9.5.0 and v.9.5.1) was used for statistical analyses. Affinity Designer (v.1.10.6) (Serif) was used to visualize data. Paired or unpaired two-tailed Student’s *t*-test, one-way ANOVA or two-way ANOVA was used to assess statistical significance, as indicated in the figure legends. Data are shown as the mean ± s.d., mean ± s.e.m. or box and whiskers plots, as indicated in the figure legends.

Reporting summary

Further information on research design is available in the Nature Portfolio Reporting Summary linked to this article.

Data availability

Data from scRNA-seq and scTCR-seq of CD8⁺ TILs and data from RNA-seq of TCF1⁺CD8⁺ T cells from in vitro T cell cultures have been deposited into the Gene Expression Omnibus (GEO); <https://www.ncbi.nlm.nih.gov/gds>) under the superseries number GSE231340 (subseries numbers GSE231301 and GSE231302). The pre-built mouse reference v2020-A was provided by 10x Genomics (downloaded from <https://cf.10xgenomics.com/supp/cell-exp/refdata-gex-GRCh38-2020-A.tar.gz>) and is based on the mm10 GRCm38.p6 release 98 from Ensembl (http://ftp.ensembl.org/pub/release-98/fasta/mus_musculus/dna/Mus_musculus.GRCm38.dna.primary_assembly.fa.gz) with reference annotation from GENCODE Release M23 (http://ftp.ebi.ac.uk/pub/databases/genocode/Genocode_mouse/release_M23/genocode.vM23.primary_assembly.annotation.gtf.gz) provided by 10x Genomics. The pre-built GRCm38 Mouse V(D)J Reference v.5.0.0 was provided by 10x Genomics and downloaded from <https://cf.10xgenomics.com/supp/cell-vdj/refdata-cellranger-vg-GRCh38-alts-ensembl-5.0.0.tar.gz>. Source data are provided with this paper.

44. Wübbenhorst, D. et al. Tetracycline-regulated bone morphogenetic protein 2 gene expression in lentivirally transduced primary rabbit chondrocytes for treatment of cartilage defects. *Arthritis Rheum.* **62**, 2037–2046 (2010).
45. Di Pilato, M. et al. Targeting the CBM complex causes T_{reg} cells to prime tumours for immune checkpoint therapy. *Nature* **570**, 112–116 (2019).
46. Oh, S. A., Seki, A. & Rutz, S. Ribonucleoprotein transfection for CRISPR/Cas9-mediated gene knockout in primary T cells. *Curr. Protoc. Immunol.* **124**, e69 (2019).
47. Labun, K. et al. CHOPCHOP v3: expanding the CRISPR web toolbox beyond genome editing. *Nucleic Acids Res.* **47**, W171–W174 (2019).
48. Doench, J. G. et al. Optimized sgRNA design to maximize activity and minimize off-target effects of CRISPR–Cas9. *Nat. Biotechnol.* **34**, 184–191 (2016).
49. Zheng, G. X. Y. et al. Massively parallel digital transcriptional profiling of single cells. *Nat. Commun.* **8**, 14049 (2017).
50. Hao, Y. et al. Integrated analysis of multimodal single-cell data. *Cell* **184**, 3573–3587.e29 (2021).
51. Hafemeister, C. & Satija, R. Normalization and variance stabilization of single-cell RNA-seq data using regularized negative binomial regression. *Genome Biol.* **20**, 296 (2019).
52. Ahlmann-Eltze, C. & Huber, W. glmGamPoi: fitting Gamma–Poisson generalized linear models on single cell count data. *Bioinformatics* **36**, 5701–5702 (2021).
53. Aran, D. et al. Reference-based analysis of lung single-cell sequencing reveals a transitional profibrotic macrophage. *Nat. Immunol.* **20**, 163–172 (2019).
54. Gattinoni, L. et al. A human memory T cell subset with stem cell-like properties. *Nat. Med.* **17**, 1290–1297 (2011).
55. Love, M. I., Huber, W. & Anders, S. Moderated estimation of fold change and dispersion for RNA-seq data with DESeq2. *Genome Biol.* **15**, 550 (2014).
56. Kaech, S. M., Hemby, S., Kersh, E. & Ahmed, R. Molecular and functional profiling of memory CD8 T cell differentiation. *Cell* **111**, 837–851 (2002).
57. Street, K. et al. Slingshot: cell lineage and pseudotime inference for single-cell transcriptomics. *BMC Genomics* **19**, 477 (2018).
58. Borcharding, N., Bormann, N. L. & Kraus, G. scRepertoire: an R-based toolkit for single-cell immune receptor analysis. *F1000Research* **9**, 47 (2020).
59. Badia-I-Mompel, P. et al. decoupleR: ensemble of computational methods to infer biological activities from omics data. *Bioinform. Adv.* **2**, vbac016 (2022).
60. Holland, C. H., Szalai, B. & Saez-Rodriguez, J. Transfer of regulatory knowledge from human to mouse for functional genomics analysis. *Biochim. Biophys. Acta Gene Regul. Mech.* **1863**, 194431 (2020).
61. Pedersen, T. tidygraph: A tidy API for graph manipulation. *GitHub* <https://github.com/thomasp85/tidygraph> (2023).
62. Csárdi, G. and Nepusz, T. The igraph software package for complex network research. *Gigascience* <https://doi.org/10.1093/gigascience/giab008> (2006).
63. Ramirez, F. et al. deepTools2: a next generation web server for deep-sequencing data analysis. *Nucleic Acids Res.* **44**, W160–W165 (2016).
64. Danecek, P. et al. Twelve years of SAMtools and BCFtools. *GigaScience* **10**, giab008 (2021).
65. Ou, J. & Zhu, L. J. trackViewer: a Bioconductor package for interactive and integrative visualization of multi-omics data. *Nat. Methods* **16**, 453–454 (2019).

Acknowledgements We are grateful to C. Reis e Sousa and R. Marais for sharing the BRAF^{V600E} cell lines and T. Mempel for providing D4M.3A-pOVA cells; and members of the Institute of Molecular Immunology and G. Coukos for discussions and suggestions. This work was supported by the Elite Network of Bavaria (N-LW-2016-370 awarded to J.P.B., i-Target to S.K.); the German research foundation (DFG) project numbers 424926990, 442405234, 449174900 and 461704785–SPP awarded to J.P.B., KO5055-2-1 and 510821390 to S.K., ZE 832/8-1, ZE 832/6-1 and SFB 1371 project P07 to D.Z. and SFB-TRR 338/1 2021–452881907 projects A01 (D.H.B.), B01 (S.K.), B02 (V.R.B), start-up funding (J.P.B.); the European Research Council (ERC, 756017, 101100460 and 101124203 to S.K.); and the German Cancer Aid (DKH, 70113918 to V.R.B., AvantCAR.de to S.K.); the Wilhelm-Sander Foundation to S.K.; the Else Kröner-Fresenius-Stiftung (IOLIN to S.S. and S.K.) and the Bavarian Research Foundation (BAYCELLATOR to

Article

D.H.B. and S.K.), M.M., A.J.G and D.D.J received support from the Lausanne Branch of the Ludwig Institute for Cancer Research.

Author contributions Conceptualization: S.B.L., J.D., M.M., A.J.G., V.R.B., D.Z., P.A.K., D.D.L., S.K. and J.P.B. Investigation: S.B.L., J.D., P.M., F.B., A.-M.P., A.H., J.H., L.R., T.J.R., N.S., A.O., L.G., S.L., S.M., D.B., L.F., L.M. and S.S. Formal analysis: S.B.L., J.D., G.P.d.A., P.M., F.B. and J.H. Methodology: S.B.L., J.D., S.J., G.P.d.A., D.H.B., V.R.B., D.Z., S.K. and J.P.B. Resources: G.P.d.A., D.H.B., V.R.B., P.K. and D.Z. Supervision: S.K. and J.P.B. Writing: S.B.L., J.D., S.K. and J.P.B. All authors contributed to feedback and proofreading.

Funding Open access funding provided by Technische Universität München.

Competing interests J.P.B., S.B.L., A.-M.P., P.K. and S.K. are preparing a patent application that includes work in this manuscript.

Additional information

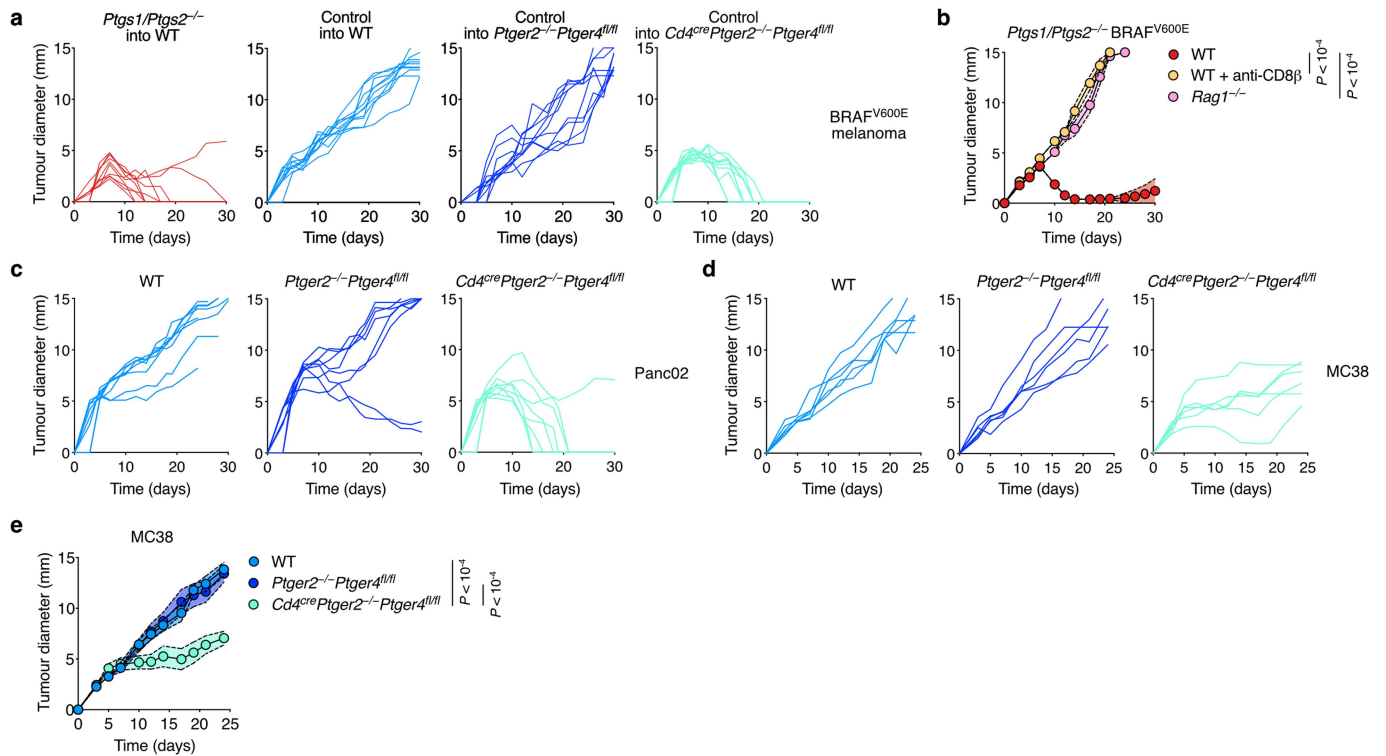
Supplementary information The online version contains supplementary material available at <https://doi.org/10.1038/s41586-024-07254-x>.

Correspondence and requests for materials should be addressed to Jan P. Böttcher.

Peer review information Nature thanks Tyler Curiel and the other, anonymous, reviewer(s) for their contribution to the peer review of this work.

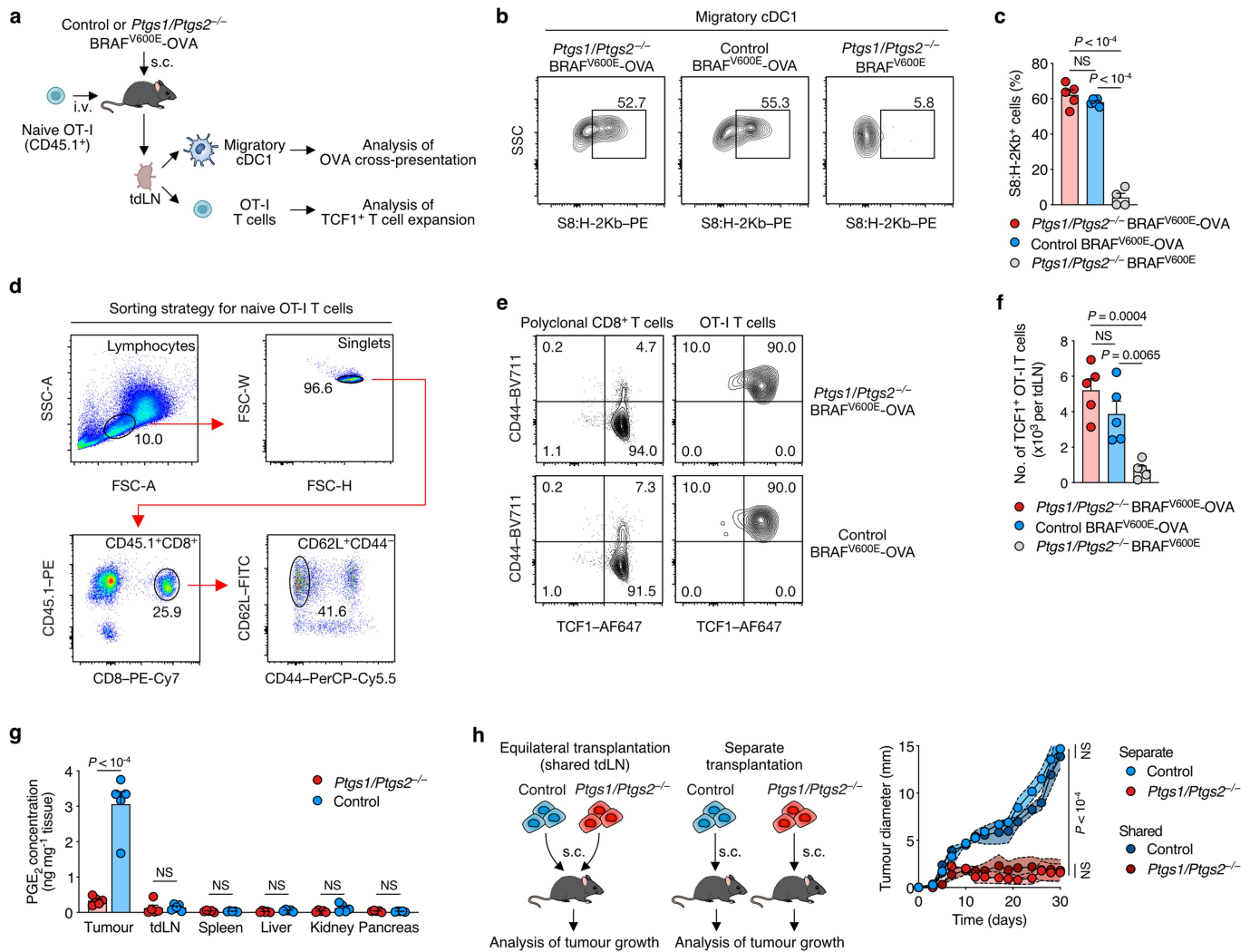
Reprints and permissions information is available at <http://www.nature.com/reprints>.

Article



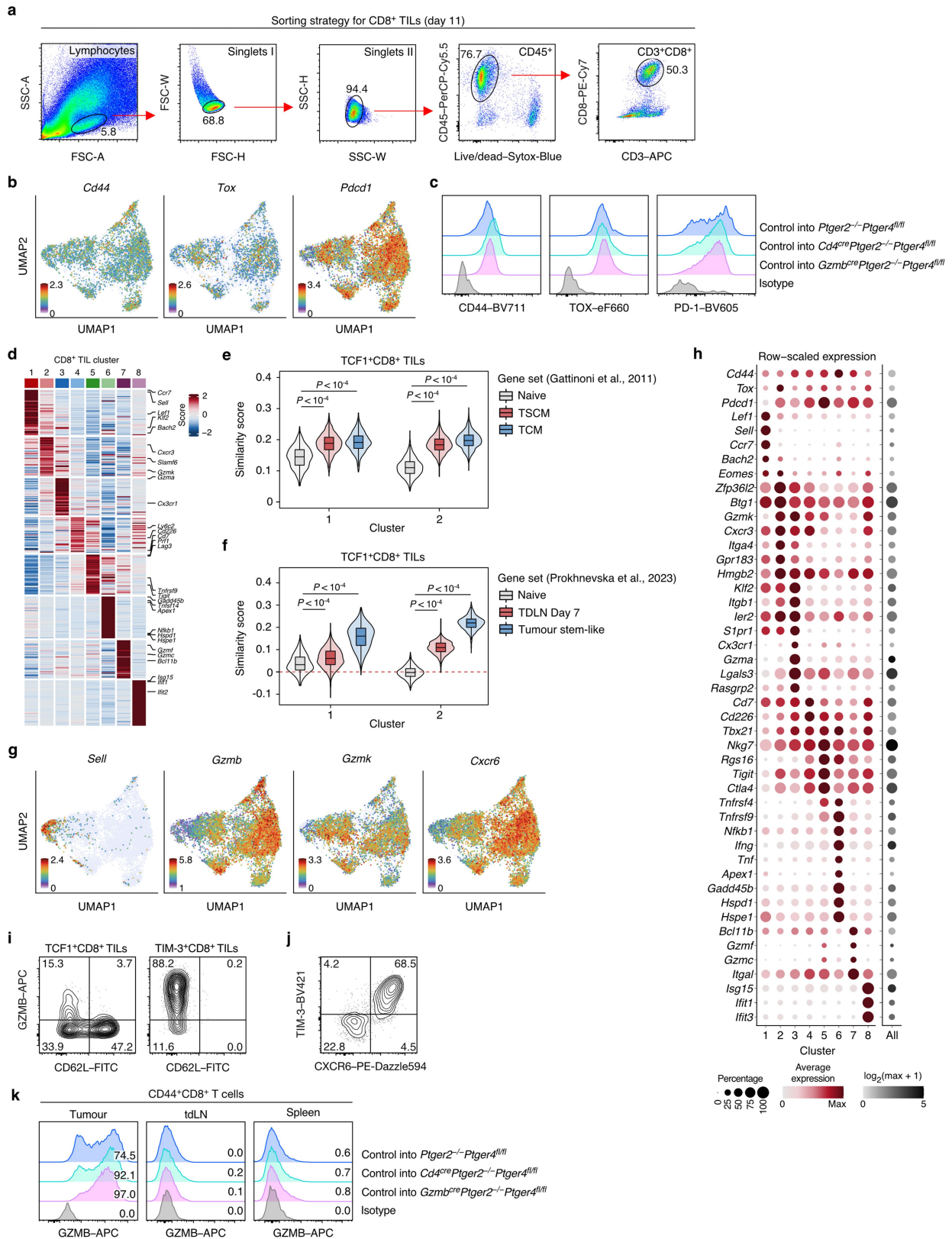
Extended Data Fig. 2 | *Cd4^{cre}Ptger2^{-/-}Ptger4^{fl/fl}* mice reject PGE₂-producing tumours. Growth profiles following s.c. inoculation of cancer cell lines into WT, *Ptger2^{-/-}Ptger4^{fl/fl}* or *Cd4^{cre}Ptger2^{-/-}Ptger4^{fl/fl}* mice. **a**, Individual profiles of 2×10^5 control or *Ptgs1/Ptgs2^{-/-}* BRAF^{V600E} tumour cells (n = 10). **b**, Growth of 2×10^5 *Ptgs1/Ptgs2^{-/-}* BRAF^{V600E} melanoma cells transplanted into *Rag1^{-/-}* mice (n = 4) or WT mice with or without CD8⁺ T cell depletion (n = 5 per group).

c, Individual profiles of 2×10^6 Panc02 tumour cells (n = 8). **d**, Individual profiles of 2×10^5 MC38 tumour cells (n = 6). **e**, Representation of all profiles shown in **d**. Data in **a-e** are pooled from two (**b,c,d,e**) or three (**a**) independent experiments and depicted as mean \pm s.e.m. P values are from two-way ANOVA with Bonferroni's multiple-comparison test. $P \geq 0.05$, not significant (NS).



Extended Data Fig. 3 | Tumour-derived PGE₂ does not impact on priming of anticancer CD8⁺ T cells in lymph nodes. **a**, Experimental design for **b–e**. WT mice received 1×10^3 naive OVA-specific CD45.1⁺ OT-I T cells followed by inoculation with 2×10^6 control or *Ptgs1/Ptgs2*^{-/-} BRAF^{V600E}-OVA cells. 6 days later, tdLNs were analysed by flow cytometry. Mice injected with *Ptgs1/Ptgs2*^{-/-} BRAF^{V600E} cells (lacking OVA expression) served as control. **b**, Representative plot showing S8:H-2K^b surface staining on migratory cDC1 (identified as live CD45⁺CD11c⁺MHCII^{hi}CD103⁺CD8 α ⁻CD11b⁻ cells). **c**, Quantification based on **b**, with $n = 5$ for control and *Ptgs1/Ptgs2*^{-/-} BRAF^{V600E}-OVA, $n = 4$ for *Ptgs1/Ptgs2*^{-/-} BRAF^{V600E}. **d**, Flow cytometry plots showing the sorting strategy for naive OT-I T cells. **e**, Flow cytometry plots showing expression of CD44 and TCF1 in polyclonal CD8⁺ T cells and OVA-specific OT-I T cells. **f**, Quantification

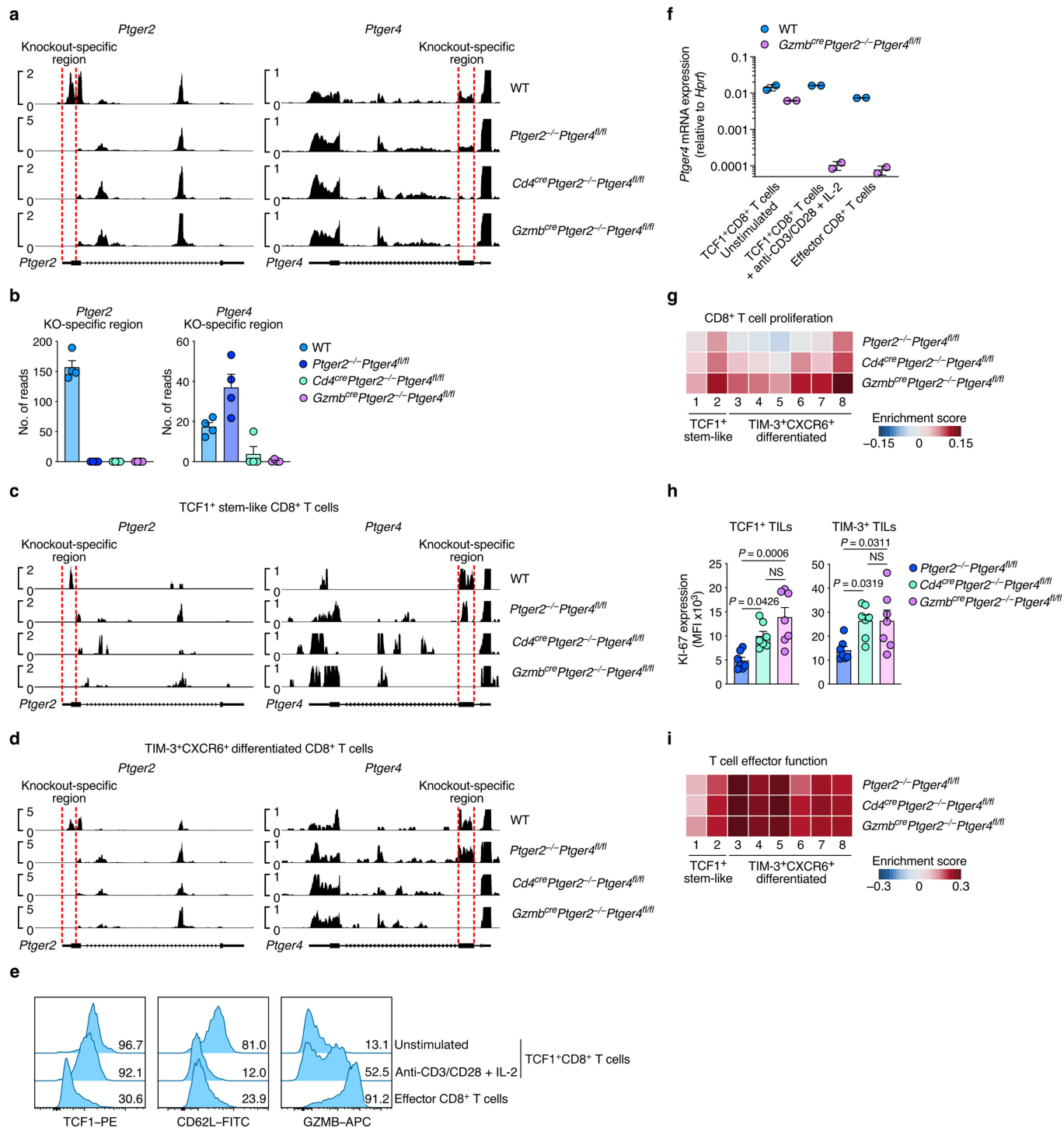
of antigen-experienced CD44⁺ TCF1⁺ OT-I T cells based on **e**, $n = 5$. **g**, PGE₂ concentration in lysates from tumours and indicated organs analysed 11 days after s.c. inoculation of WT mice with control or *Ptgs1/Ptgs2*^{-/-} BRAF^{V600E} melanoma cells ($n = 5$ per group). **h**, Effect of equilateral co-transplantation of 2×10^5 control and *Ptgs1/Ptgs2*^{-/-} BRAF^{V600E} tumours on tumour growth ($n = 4$ per group). Data in **c** and **f–h** are pooled from two (**c, f, h**) or three (**g**) independent experiments and depicted as mean \pm s.e.m. Plots in **b, e** show data for one sample representative for $n = 5$ samples from two independent experiments. *P* values in **c, f** are from one-way ANOVA with Tukey's multiple-comparison test, *P* values in **g** are from unpaired t-tests, *P* values in **h** are from two-way ANOVA with Bonferroni's multiple-comparison test. $P \geq 0.05$, not significant (NS).



Extended Data Fig. 4 | See next page for caption.

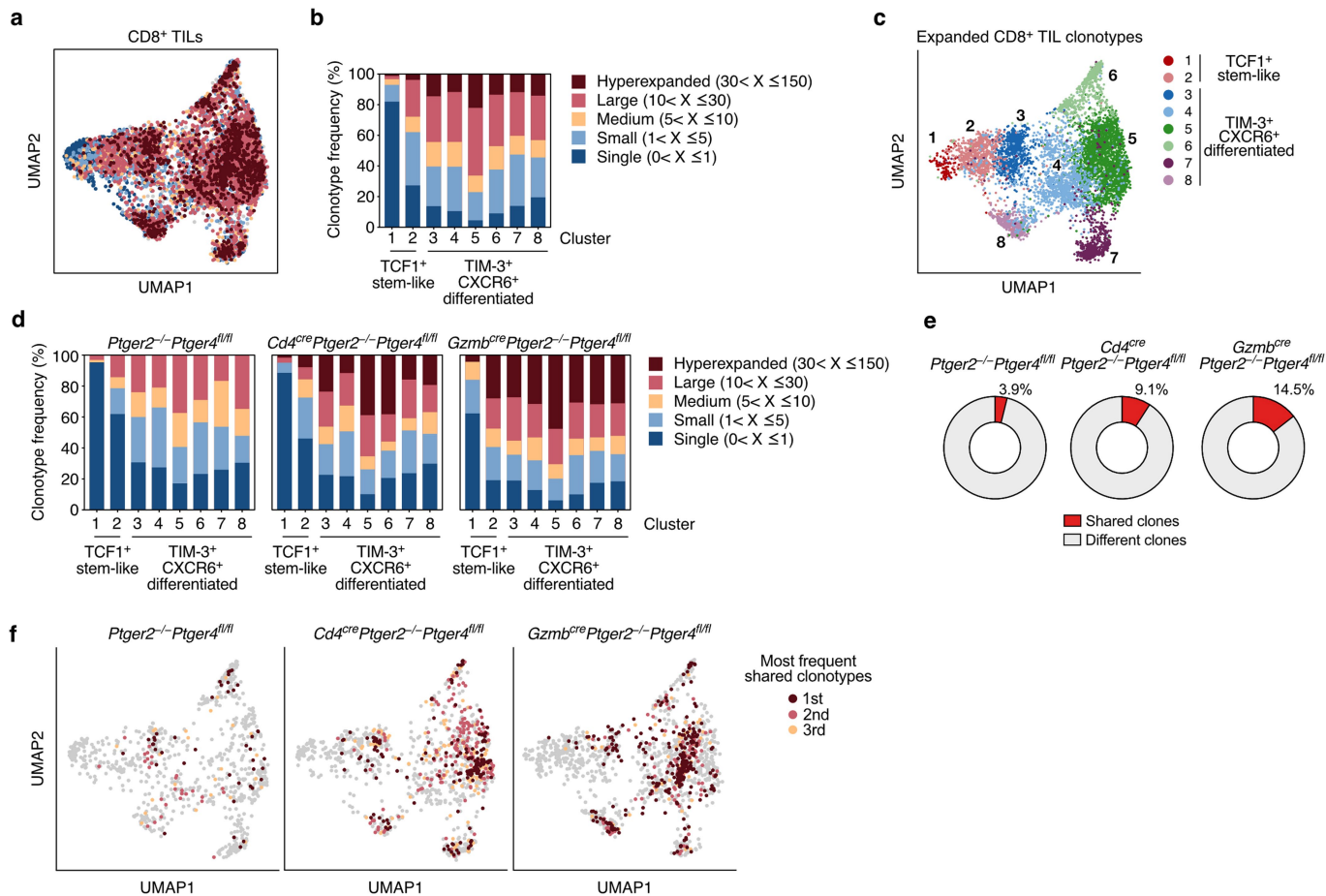
Extended Data Fig. 4 | Isolation of CD8⁺ TILs for scRNA-seq and phenotypic characterisation of CD8⁺ TIL populations. *Ptger2*^{-/-}*Ptger4*^{fl/fl}, *Cd4*^{cre}*Ptger2*^{-/-}*Ptger4*^{fl/fl} or *Gzmb*^{cre}*Ptger2*^{-/-}*Ptger4*^{fl/fl} mice were transplanted with 2 × 10⁶ control BRAF^{V600E} melanoma cells. After 11 days, CD8⁺ TIL populations were sorted from n = 4 tumours per group and analysed by scRNA-seq (**b,d-h**) or flow cytometry (**c,i-k**). **a**, Flow cytometry plots showing the sorting strategy. **b**, UMAP plots showing transcript expression of *Cd44*, *Tox* and *Pdcd1* (encoding PD-1) as determined by scRNA-seq. **c**, Flow cytometric analysis of CD44, TOX and PD-1 protein expression in CD8⁺ TILs. **d**, Heatmap showing the expression of cluster signature transcripts (top 50). **e,f**, Correlation of TCF1⁺CD8⁺ TIL cluster gene expression with gene signatures of **e** naive CD8⁺ T cells, memory stem cell CD8⁺ T cells (TSCM) and central memory CD8⁺ T cells (TCM) or **f** naive CD8⁺ T cells, tumour antigen-specific CD8⁺ T cells in tDLNs and tumour-infiltrating stem-like CD8⁺ T cells. **g**, UMAP

visualisation of transcript expression of indicated immune genes as determined by scRNA-seq. **h**, Expression levels of selected immune genes across CD8⁺ TIL clusters. **i**, Flow cytometric analysis of GZMB and CD62L expression among TCF1⁺ and TIM-3⁺ CD8⁺ TIL populations from a WT mouse. **j**, Flow cytometric analysis of TIM-3 and CXCR6 protein expression in CD8⁺ TILs from a WT mouse. **k**, Analysis of GZMB expression in activated (CD44⁺) CD8⁺ T cells isolated from tumours, tDLNs and spleen. Numbers indicate percentage of GZMB⁺ cells compared to isotype control. Plots in **a,c,i-k** show data for one tumour representative for n = 6 tumours from one (**a,b**), two (**c,i,k**), or three (**j**) independent experiments or pooled data from n = 4 biological replicates from one experiment (**d-h**). *P* values in **e,f** are from pairwise comparisons using Wilcoxon rank sum test and Bonferroni correction for multiple testing. *P* ≥ 0.05, not significant (NS).



Extended Data Fig. 5 | *Gzmb^{cre}Ptger2^{-/-}Ptger4^{fl/fl}* mice exhibit *Ptger4* knockout in TCF1⁺ CD8⁺ TILs; increased proliferation of TCF1⁺ CD8⁺ TILs and their progeny in T cell-specific EP₂/EP₄ double deficient mice. a, Gene tracks showing the average scRNA-seq read coverage on *Ptger2* and *Ptger4* loci in CD8⁺ TILs from BRAF^{V600E} melanoma tumours in WT, *Ptger2^{-/-}Ptger4^{fl/fl}*, *Cd4^{cre}Ptger2^{-/-}Ptger4^{fl/fl}* and *Gzmb^{cre}Ptger2^{-/-}Ptger4^{fl/fl}* mice across all replicates. Dashed boxes highlight knockout(KO)-specific target regions. **b**, Quantification of *Ptger2* and *Ptger4* read coverage for KO-specific target regions based on **a**. n = 4. **c,d**, Gene tracks showing the scRNA-seq read coverage on *Ptger2* and *Ptger4* loci in **c**, TCF1⁺ CD8⁺ TILs and **d**, TIM-3⁺ TIL progeny from WT, *Ptger2^{-/-}Ptger4^{fl/fl}*, *Cd4^{cre}Ptger2^{-/-}Ptger4^{fl/fl}* and *Gzmb^{cre}Ptger2^{-/-}Ptger4^{fl/fl}* mice. Data for one representative replicate with comparable cell numbers is shown. **e,f**, WT or *Gzmb^{cre}Ptger2^{-/-}Ptger4^{fl/fl}* TCF1⁺ stem-like and TCF1⁺ effector CD8⁺ T cells from in vitro T cell cultures were stimulated or not with anti-CD3/CD28 for 24 h.

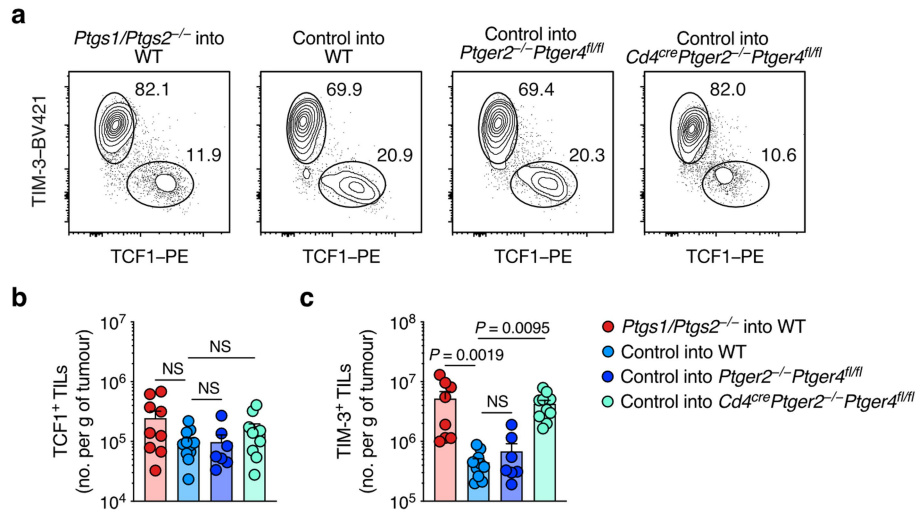
e, Representative flow cytometry plots showing TCF1, CD62L and GZMB protein expression. **f**, *Ptger4* mRNA expression as measured by knock-out sensitive RT-PCR (n = 2). **g**, Expression of a CD8⁺ T cell proliferation signature across the distinct populations of CD8⁺ TILs from *Ptger2^{-/-}Ptger4^{fl/fl}*, *Cd4^{cre}Ptger2^{-/-}Ptger4^{fl/fl}* and *Gzmb^{cre}Ptger2^{-/-}Ptger4^{fl/fl}* mice based on scRNA-seq. **h**, Analysis of Ki-67 protein expression in TCF1⁺ and TIM-3⁺ CD8⁺ TILs 11 days after inoculation of *Ptger2^{-/-}Ptger4^{fl/fl}*, *Cd4^{cre}Ptger2^{-/-}Ptger4^{fl/fl}* and *Gzmb^{cre}Ptger2^{-/-}Ptger4^{fl/fl}* mice with 2 × 10⁶ control BRAF^{V600E} melanoma cells. n = 7. **i**, Expression of a gene signature for T cell effector function, analysed as in **g**. Data in **a-e,g,i** are from one experiment. Data in **b,h** are pooled from two (**b**) or three (**h**) independent experiments and depicted as mean ± s.e.m. Data in **f** are depicted as mean ± s.d. from one experiment. P values are from one-way ANOVA with Tukey's multiple-comparison test. P ≥ 0.05, not significant (NS).



Extended Data Fig. 6 | EP₂/EP₄ double deficiency permits clonal differentiation and expansion of CD8⁺ TILs in PGE₂-producing tumours.

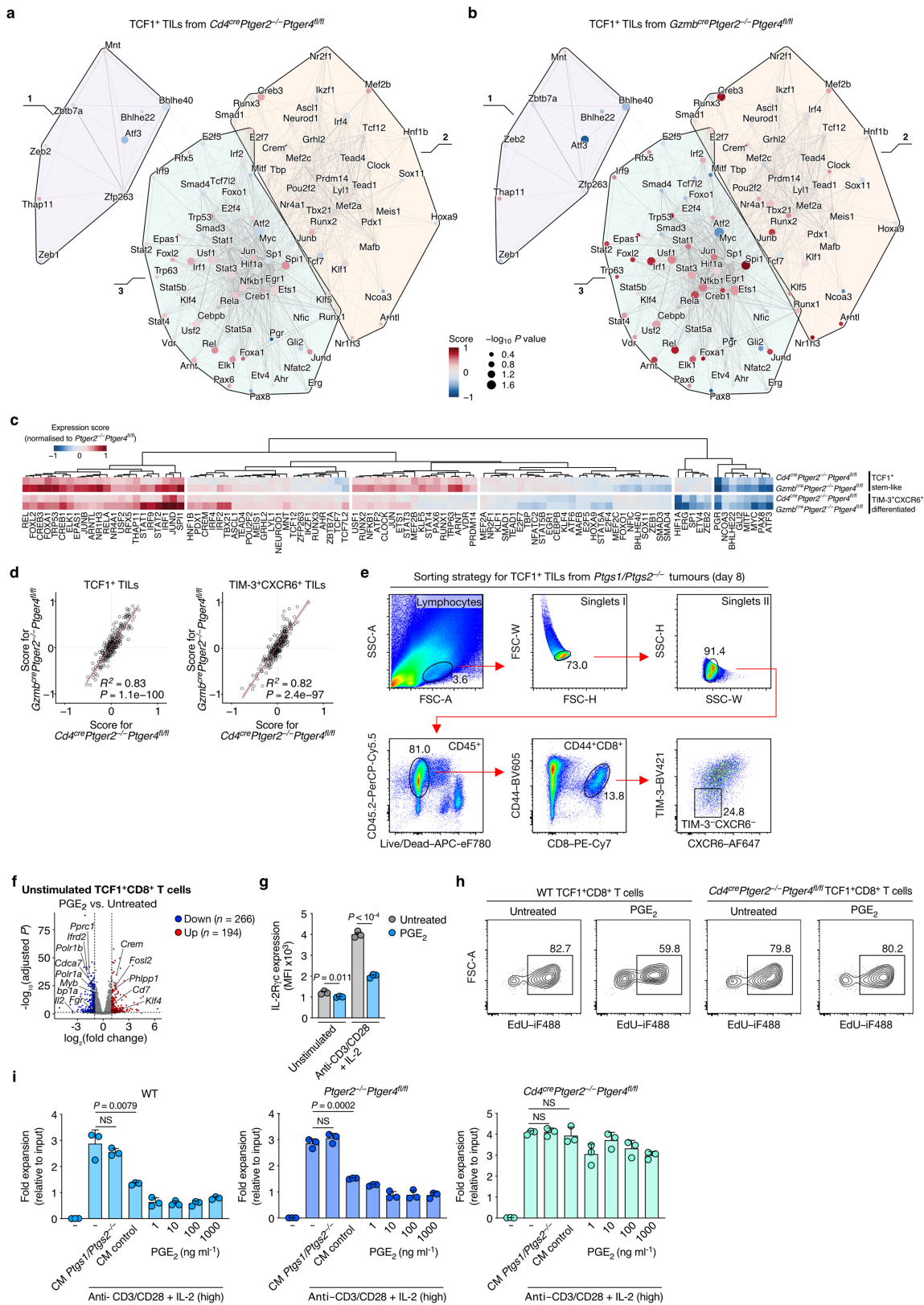
a, UMAP visualisations of T cell clonotype distribution across CD8⁺ TILs based on scTCR-seq. **b**, Clonotype frequency across CD8⁺ TIL clusters based on **a**. **c**, UMAP visualisation of expanded tumour-infiltrating CD8⁺ T cell clonotypes coloured according to cluster classification. **d**, Comparison of clonotype

frequencies between *Ptger2*^{-/-}*Ptger4*^{fl/fl}, *Cd4*^{cre}*Ptger2*^{-/-}*Ptger4*^{fl/fl} and *Gzmb*^{cre}*Ptger2*^{-/-}*Ptger4*^{fl/fl} mice. **e**, Frequencies of T cell clones shared between TCF1⁺CD8⁺ TILs and TIM-3⁺ TIL progeny. **f**, UMAP plots visualising the top 3 most frequent shared clonotypes for *Ptger2*^{-/-}*Ptger4*^{fl/fl}, *Cd4*^{cre}*Ptger2*^{-/-}*Ptger4*^{fl/fl} and *Gzmb*^{cre}*Ptger2*^{-/-}*Ptger4*^{fl/fl} mice. Data are from one experiment.



Extended Data Fig. 7 | EP₂/EP₄ double deficiency rescues development of early and terminally differentiated effector CD8⁺ T cells within tumour tissue. **a-c**, WT, *Ptger2*^{-/-}*Ptger4*^{fl/fl} or *Cd4*^{cre}*Ptger2*^{-/-}*Ptger4*^{fl/fl} mice were injected s.c. with 2×10⁶ control or *Ptgs1/Ptgs2*^{-/-} BRAF^{V600E} cells and CD44⁺CD8⁺ TILs were analysed 11 days later by flow cytometry. **a**, Representative plots showing the frequency of TCF1⁺ stem-like and TIM-3⁺ effector CD8⁺ TIL populations. **b**, Quantification of TCF1⁺CD8⁺ TILs (*Ptgs1/Ptgs2*^{-/-} into WT, n = 9; Control into WT, n = 11; Control into *Ptger2*^{-/-}*Ptger4*^{fl/fl}, n = 7; Control into *Cd4*^{cre}*Ptger2*^{-/-}*Ptger4*^{fl/fl},

n = 10). **c**, Quantification of TIM-3⁺CD8⁺ TILs (*Ptgs1/Ptgs2*^{-/-} into WT, n = 8; Control into WT, n = 10; Control into *Ptger2*^{-/-}*Ptger4*^{fl/fl}, n = 7; Control into *Cd4*^{cre}*Ptger2*^{-/-}*Ptger4*^{fl/fl}, n = 10). Data in **b,c** are pooled from three independent experiments and depicted as mean ± s.e.m. Plots in **a** show data for one tumour sample representative for at least n = 7 samples from three independent experiments. *P* values are from one-way ANOVA with Tukey's multiple-comparison test. *P* ≥ 0.05, not significant (NS).

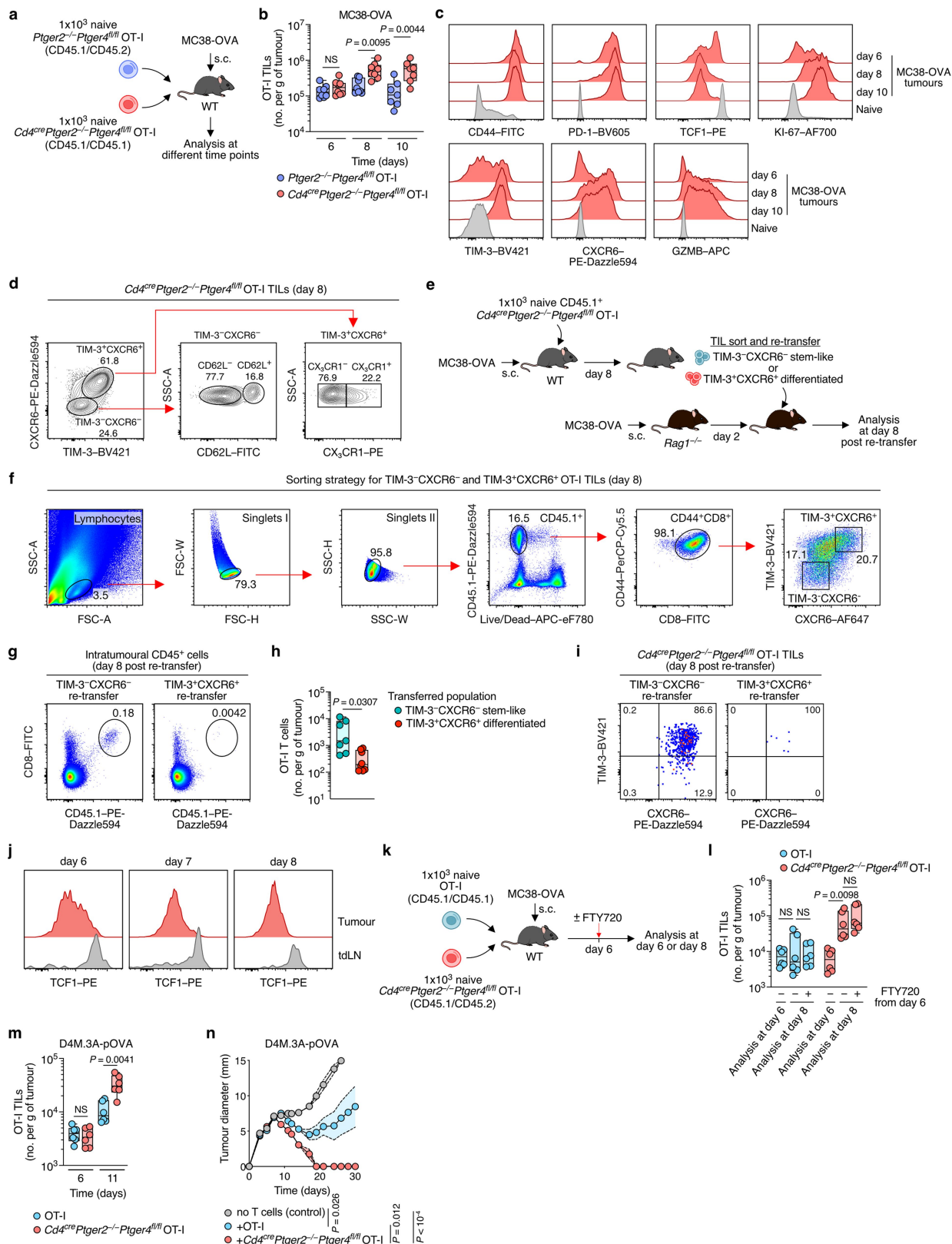


Extended Data Fig. 8 | See next page for caption.

Article

Extended Data Fig. 8 | PGE₂-mediated changes in TCF1⁺CD8⁺ T cells, effect on γ c expression and proliferation. a-d, scRNA-seq based analysis of TF activity alterations in TCF1⁺CD8⁺ TILs and their TIM-3⁺CXCR6⁺ effector progeny between control BRAF^{V600E} melanoma tumours in *Cd4^{cre}Ptger2^{-/-}Ptger4^{fl/fl}* and *Gzmb^{cre}Ptger2^{-/-}Ptger4^{fl/fl}* mice compared to *Ptger2^{-/-}Ptger4^{fl/fl}* mice. **a,b**, Alterations of TF network activity in TCF1⁺CD8⁺ TILs from BRAF^{V600E} melanoma tumours in **a**, *Cd4^{cre}Ptger2^{-/-}Ptger4^{fl/fl}* mice compared to *Ptger2^{-/-}Ptger4^{fl/fl}* mice or **b**, *Gzmb^{cre}Ptger2^{-/-}Ptger4^{fl/fl}* mice compared to *Ptger2^{-/-}Ptger4^{fl/fl}* mice. **c**, Heatmap visualisation, **d**, Correlation of TF activity alterations for TIL populations from *Cd4^{cre}Ptger2^{-/-}Ptger4^{fl/fl}* and *Gzmb^{cre}Ptger2^{-/-}Ptger4^{fl/fl}* mice. **e**, Flow cytometry plots showing the sorting strategy for TCF1⁺ TILs (identified as TIM-3⁻CXCR6⁻ cells) from *Ptgs1/Ptgs2^{-/-}* BRAF^{V600E} tumours. **f**, Volcano plot showing the effect of PGE₂ exposure on gene expression in TCF1⁺CD8⁺ T cells from in vitro T cell cultures, based on RNA-seq analysis.

g, Effect of PGE₂ treatment on IL-2R γ c protein expression (n = 3). **h**, WT or *Cd4^{cre}Ptger2^{-/-}Ptger4^{fl/fl}* TCF1⁺CD8⁺ T cells from in vitro T cell cultures were stimulated with anti-CD3/CD28 and high-dose IL-2 in presence or absence of PGE₂. After 24 h cells were analysed for T cell proliferation by EdU incorporation. **i**, WT, *Ptger2^{-/-}Ptger4^{fl/fl}* or *Cd4^{cre}Ptger2^{-/-}Ptger4^{fl/fl}* TCF1⁺CD8⁺ T cells were treated or not with tumour cell conditioned medium (CM) or PGE₂ and stimulated as indicated. After 72 h, T cell expansion was analysed by flow cytometry. n = 3. Data in **a-d**, **f** are from one experiment. Data in **g,i** show data for one representative of two independent experiments with n = 3 biological replicates. In **f**, DEGs ($P < 0.05$; fold change ≥ 2) were identified by Wald test with multiple testing by the Benjamini-Hochberg method. Horizontal lines and error bars in **(g,i)** indicate mean \pm s.d. P -values are from **d**, Fitted linear regression models or **g**, and **i**, unpaired t-test. $P \geq 0.05$, not significant (NS). Plots in **(h)** show data for one sample representative for n = 3 samples.



Extended Data Fig. 9 | See next page for caption.

Article

Extended Data Fig. 9 | PGE₂ impairs proliferative expansion and effector differentiation of antigen-specific TCF1⁺CD8⁺ TILs. **a**, Experimental design for **b-d**. **b**, Quantification of OT-I cell expansion in tumours at different time points (day 6 and day 8: n = 8 per group; day 10: n = 7 per group). **c**, Histograms showing expression of indicated molecules in *Cd4^{cre}Ptger2^{-/-}Ptger4^{fl/fl}* OT-I TILs at different time points. Naive *Cd4^{cre}Ptger2^{-/-}Ptger4^{fl/fl}* OT-I T cells served as control. **d**, Flow cytometry plots showing subpopulation composition among *Cd4^{cre}Ptger2^{-/-}Ptger4^{fl/fl}* OT-I TILs. **e-h**, WT mice received 1×10^3 naive congenically marked CD45.1⁺ *Cd4^{cre}Ptger2^{-/-}Ptger4^{fl/fl}* OT-I T cells followed by inoculation with 2×10^6 MC38-OVA cells. 8 days later, the indicated subpopulations of OT-I TILs were sorted and 7×10^3 cells were re-transferred into MC38-OVA bearing *Rag1^{-/-}* recipient mice. TILs in *Rag1^{-/-}* recipients were analysed at day 8 post re-transfer. **e**, Experimental design. **f**, Flow cytometry plots showing the sorting strategy. **g**, Flow cytometry plots showing the frequency of OT-I TILs recovered at day 8 post re-transfer. **h**, Quantification of OT-I TIL progenies based on (**g**), with TIM-3⁺CXCR6⁻ stem-like, n = 7; TIM-3⁺CXCR6⁺ differentiated, n = 8. **i**, Flow cytometry plots showing the expression of TIM-3 and CXCR6 among recovered

OT-I TILs. **j**, Analysis of TCF1 expression in *Cd4^{cre}Ptger2^{-/-}Ptger4^{fl/fl}* OT-I T cells in tdLNs and tumours over time. **k**, Experimental design for **l**. **l**, Effect of FTY720 treatment from day 6 on OT-I T cell expansion in tumours (n = 6). **m, n**, WT mice received 1×10^3 naive OT-I T cells or 1×10^3 naive *Cd4^{cre}Ptger2^{-/-}Ptger4^{fl/fl}* OT-I T cells i.v. and were transplanted s.c. with 2×10^6 D4M.3A-pOVA melanoma cells before **m**, quantification of OT-I cell expansion in tumours at different time points (n = 6) or **n**, analysis of tumour growth over time (n = 4). Data in **b, h, l-n** are pooled from two (**h, l-n**) or three (**b**) independent experiments and depicted as box plots extending from the 25th to 75th percentiles with the median as centre and whiskers corresponding to minimum and maximum values (**b, h, l, m**) or shown as mean \pm s.e.m. (**n**). Plots in **c, d, g, i, j** show data for one sample representative for (**c, d, g, i**) n = 7 or (**j**) n = 6 samples from two independent experiments. *P* values in **b, l** are from one-way ANOVA with Tukey's multiple-comparison test, *P* values in **h, m** are from unpaired t-test, *P* values in **n** are from two-way ANOVA with Bonferroni's correction for multiple testing. *P* \geq 0.05, not significant (NS).

Reporting Summary

Nature Portfolio wishes to improve the reproducibility of the work that we publish. This form provides structure for consistency and transparency in reporting. For further information on Nature Portfolio policies, see our [Editorial Policies](#) and the [Editorial Policy Checklist](#).

Statistics

For all statistical analyses, confirm that the following items are present in the figure legend, table legend, main text, or Methods section.

n/a | Confirmed

- The exact sample size (n) for each experimental group/condition, given as a discrete number and unit of measurement
- A statement on whether measurements were taken from distinct samples or whether the same sample was measured repeatedly
- The statistical test(s) used AND whether they are one- or two-sided
Only common tests should be described solely by name; describe more complex techniques in the Methods section.
- A description of all covariates tested
- A description of any assumptions or corrections, such as tests of normality and adjustment for multiple comparisons
- A full description of the statistical parameters including central tendency (e.g. means) or other basic estimates (e.g. regression coefficient) AND variation (e.g. standard deviation) or associated estimates of uncertainty (e.g. confidence intervals)
- For null hypothesis testing, the test statistic (e.g. F , t , r) with confidence intervals, effect sizes, degrees of freedom and P value noted
Give P values as exact values whenever suitable.
- For Bayesian analysis, information on the choice of priors and Markov chain Monte Carlo settings
- For hierarchical and complex designs, identification of the appropriate level for tests and full reporting of outcomes
- Estimates of effect sizes (e.g. Cohen's d , Pearson's r), indicating how they were calculated

Our web collection on [statistics for biologists](#) contains articles on many of the points above.

Software and code

Policy information about [availability of computer code](#)

Data collection

Flow cytometer data was collected on a LSRFortessa Cell Analyzer using BD FACSDiva Software v8.0.1 and v9.0.1 (BD Biosciences), a SP6800 using SP6800 Spectral Analyzer Software v2.0.2.14140 (SONY Biotechnology) or a SA3800 Spectral Analyzer using SA3800 Spectral Analyzer Software v2.0.5.54250 (SONY Biotechnology). Fluorescence activated cell sorting of T cells was performed on a SH800 Cell Sorter using SH800 Cell Sorter v2.1.6 (SONY Biotechnology) or a BD FACSAria III Cell Sorter using BD FACSDiva v9.0.1.

qRT-PCR was performed on a LightCycler 48 (Roche) using LightCycler 480 Software v1.51.

PGE2 concentrations were measured on a Berthold Tristar 3 using MikroWin v5.24.

Bulk RNA was isolated using Total RNA Miniprep (Monarch).
Bulk RNA sequencing was performed using the NovaSeq6000 (Illumina).

Single-cell RNA was isolated using the Chromium Next GEM Single Cell 5' Reagent Kits v2 User Guide with Feature Barcode technology for Cell Surface Protein (Rev D).
Single-cell RNA sequencing was performed using the NovaSeq6000 (Illumina).

Data analysis

The following softwares were used for data analysis:

Flow cytometry data: FACSDiva v8.0.1 and v9.0.1 (BD Biosciences), Flowjo v00.8.1 and v10.8.2 (BD Biosciences), SH800 Cell Sorter Software (SONY Biotechnology), SP6800 Spectral Cell Analyzer Software v2.0.2.14140 (SONY Biotechnology)

Data processing, visualisation and statistical analyses: Prism v9.5.0 and v9.5.1 (GraphPad), Excel v16.82 (Microsoft), Affinity Designer v1.10.6 (Serif)

RNA-seq: Reads were aligned using the Hisat2 v2.0.5, R v4.0.4 with the R packages: DESeq2 v1.20.0 and v1.36, featureCounts v1.5.0-p3, ggplot2 v3.4.2, ggrepel 0.9.3; GSEA: The PreRanked tool from GSEA v4.3.2 was used.

scRNA-seq and scTCR-seq: Cell Ranger v6.1.1, R v4.0.4 and R v4.2.1 with the R packages: Seurat v4.0.1 and v4.1.1, sctransform v0.3.2, slingshot v2.4.0, singleR v1.10.0, scRepertoire v1.6.0, decoupleR v2.2.2, dorothea v1.8.0, tidygraph v1.2.1, deepTools v3.5.4, samtools v1.13, trackViewer v1.32.1, and igraph v1.3.2. For the scRNA-seq: NovaSeq600 platform (S4 v1.5, Illumina).

For further details please see methods section.

For manuscripts utilizing custom algorithms or software that are central to the research but not yet described in published literature, software must be made available to editors and reviewers. We strongly encourage code deposition in a community repository (e.g. GitHub). See the Nature Portfolio [guidelines for submitting code & software](#) for further information.

Data

Policy information about [availability of data](#)

All manuscripts must include a [data availability statement](#). This statement should provide the following information, where applicable:

- Accession codes, unique identifiers, or web links for publicly available datasets
- A description of any restrictions on data availability
- For clinical datasets or third party data, please ensure that the statement adheres to our [policy](#)

Data from single-cell RNA sequencing and single-cell TCR sequencing of tumour-infiltrating CD8+ T cells and data from RNA sequencing of TCF1+CD8+ T cells from in vitro T cell cultures is deposited at GEO under the SuperSeries GSE231340. This SuperSeries is composed of the following SubSeries:

GSE231301: RNA sequencing of TCF1+CD8+ T cells from in vitro T cell cultures

GSE231302: Single-cell RNA-sequencing and single-cell TCR-sequencing of tumour-infiltrating CD8+ T cells derived from mouse BRAFV600E melanoma [scRNA-Seq + TCR 10x]

The pre-built mouse reference v2020-A was provided by 10X Genomics, downloaded from <https://cf.10xgenomics.com/supp/cell-exp/refdata-gex-GRCh38-2020-A.tar.gz> and is based on the mm10 GRCh38.p6 release 98 from Ensembl (http://ftp.ensembl.org/pub/release-98/fasta/mus_musculus/dna/Mus_musculus.GRCm38.dna.primary_assembly.fa.gz) with reference annotation from GENCODE Release M23 (http://ftp.ebi.ac.uk/pub/databases/genCODE/Gencode_mouse/release_M23/genocode.vM23.primary_assembly.annotation.gtf.gz) provided by 10x Genomics). The pre-built GRCh38 Mouse V(D)J Reference v5.0.0 was provided by 10X Genomics and downloaded from <https://cf.10xgenomics.com/supp/cell-vdj/refdata-cellranger-vg-GRCh38-alts-ensembl-5.0.0.tar.gz>. Mathematical code for scRNA-seq, scTCR-seq and RNA-seq data analysis are available from the corresponding author upon reasonable request.

Human research participants

Policy information about [studies involving human research participants and Sex and Gender in Research](#).

Reporting on sex and gender

Population characteristics

Recruitment

Ethics oversight

Note that full information on the approval of the study protocol must also be provided in the manuscript.

Field-specific reporting

Please select the one below that is the best fit for your research. If you are not sure, read the appropriate sections before making your selection.

- Life sciences Behavioural & social sciences Ecological, evolutionary & environmental sciences

For a reference copy of the document with all sections, see [nature.com/documents/nr-reporting-summary-flat.pdf](https://www.nature.com/documents/nr-reporting-summary-flat.pdf)

Life sciences study design

All studies must disclose on these points even when the disclosure is negative.

Sample size

In order to determine appropriate sample sizes, we performed pilot experiments and referred to previously published results using the same or similar experimental models (Böttcher et al., 2018; Zelenay et al., 2015). No statistical methods were used to predetermine sample size. The exact n numbers for biological replicates used in the study are indicated in the respective figure legends.

Data exclusions

Every mouse designated for the respective experiment was included in the analysis. For flow cytometry, every tumour palpable at the analysis time point was analysed. Data on individual samples were excluded if any obvious problems during sample processing occurred, i.e. more

than 70% of dead cells identified by live dead staining. For scTCR-sequencing, sequencing for one replicate group failed and was therefore excluded from the analysis.

Replication

All animal experiments in this study were repeated and validated as stated in the respective figure legends.
All other experiments in this study, including ex vivo experiments, were repeated and validated as stated in the respective figure legends.
All attempts at replication were successful.

Randomization

Age- and sex-matched mice were randomly allocated into different groups and received the appropriate treatment at the same time point for comparative analyses. For experiments other than mice, every treatment condition included all samples, randomization was therefore not relevant.

Blinding

For mouse tumour experiments including Ptgs1/Ptgs2-/- BRAFV600E tumours as well as T cell depletion, investigators could not be blinded due to the overt differences in tumour size and weight, which reflected previously reported effects of these treatments in equal or similar experimental settings (Böttcher et al., Cell 2018). All other experiments were conducted in a blinded manner.
Every experiment was performed using several control samples and the applied analysis strategy (Immunofluorescence stainings, FACS gating) was identical for every single sample.

Reporting for specific materials, systems and methods

We require information from authors about some types of materials, experimental systems and methods used in many studies. Here, indicate whether each material, system or method listed is relevant to your study. If you are not sure if a list item applies to your research, read the appropriate section before selecting a response.

Materials & experimental systems

n/a	Included in the study
<input type="checkbox"/>	<input checked="" type="checkbox"/> Antibodies
<input type="checkbox"/>	<input checked="" type="checkbox"/> Eukaryotic cell lines
<input checked="" type="checkbox"/>	<input type="checkbox"/> Palaeontology and archaeology
<input type="checkbox"/>	<input checked="" type="checkbox"/> Animals and other organisms
<input checked="" type="checkbox"/>	<input type="checkbox"/> Clinical data
<input checked="" type="checkbox"/>	<input type="checkbox"/> Dual use research of concern

Methods

n/a	Included in the study
<input checked="" type="checkbox"/>	<input type="checkbox"/> ChIP-seq
<input type="checkbox"/>	<input checked="" type="checkbox"/> Flow cytometry
<input checked="" type="checkbox"/>	<input type="checkbox"/> MRI-based neuroimaging

Antibodies

Antibodies used

The following antibodies were used for flow cytometry and cell sorting:
APC anti-CD3 (1:100, clone 17A2, Thermo Fisher Scientific, Cat.#: 17-0032-82), PE anti-CD4 (1:200, clone GK1.5, Biolegend, Cat.#: 100407), AF647 anti-CD4 (1:200, clone GK1.5, Biolegend, Cat.#: 100426), PerCP/Cy5.5 anti-CD4 (1:200, clone GK1.5, Biolegend, Cat.#: 100433), BV421 anti-CD8a (1:200, clone 53-6.7, Biolegend, Cat.#: 100737), FITC anti-CD8a (1:200, clone 53-6.7, Biolegend, Cat.#: 100706), PE-Dazzle594 anti-CD8a (1:200, clone 53-6.7, Biolegend, Cat.#: 100761), PE-Cy7 anti-CD8a (1:200, clone 53-6.7, Biolegend, Cat.#: 100721), BV605 anti-CD11b (1:200, clone M1/70, Biolegend, Cat.#: 101237), PE-Cy7 anti-CD11c (1:200, clone N418, Biolegend, Cat.#: 117317), BV570 anti-mouse/human-CD44 (1:100, clone IM7, Biolegend, Cat.#: 103037), BV711 anti-mouse/human-CD44 (1:100, clone IM7, Biolegend, Cat.#: 103057), FITC anti-mouse/human-CD44 (1:100, clone IM7, Biolegend, Cat.#: 103022), PerCP-Cy5.5 anti-mouse/human-CD44 (1:100, clone IM7, Biolegend, Cat.#: 103022), AF647 anti-CD45.1 (1:100, clone A20, Biolegend, Cat.#: 110720), PE anti-CD45.1 (1:100, clone A20, Biolegend, Cat.#: 110707), PE-Dazzle594 anti-CD45.1 (1:100, clone A20, Biolegend, Cat.#: 110747), PerCP/Cy5.5 anti-CD45.1 (1:100, clone A20, Biolegend, Cat.#: 110727), BV510 anti-CD45.2 (1:100, clone 104, Biolegend, Cat.#: 109837), FITC anti-CD45.2 (1:100, clone 104, Biolegend, Cat.#: 109805), PerCP-Cy5.5 anti-CD45.2 (1:100, clone 104, Biolegend, Cat.#: 109827), FITC anti-CD62L (1:100, clone MEL-14, Biolegend, Cat.#: 104405), PE-Dazzle594 anti-CD62L (1:100, clone MEL-14, Biolegend, Cat.#: 104447), FITC anti-CD103 (1:100, clone M290, BD Biosciences, Cat.#: 557494), APC anti-CD132/IL2RGc (1:100, clone TUGm2, Biolegend, Cat.#: 132307), PE-Dazzle594 anti-CD186/CXCR6 (1:200, clone SA051D1, Biolegend, Cat.#: 151116), PE anti-CX3CR1 (1:100, clone SA011F11, Biolegend, Cat.#: 149006), BV605 anti-CD279/PD-1 (1:100, clone 29F.1A12, Biolegend, Cat.#: 135219), BV421 anti-CD366/TIM-3 (1:200, clone RMT3-23, Biolegend, Cat.#: 119723), PerCP/Cy5.5 anti-TCRb (1:100, clone H57-597, Biolegend, Cat.#: 109227), AF700 anti-I-A/I-E (MHC class II) (1:500, clone M5/114.15.2, Biolegend, Cat.#: 107621), PE anti-H-2Kb bound to SIINFEKL (1:100, clone 25-D1.16, Biolegend, Cat.#: 141603), APC anti-human Granzyme B (1:200, clone GB12, Thermo Fisher Scientific, Cat.#: MHGB05), FITC anti-Ki-67 (1:100, clone SolA-15, Thermo Fisher Scientific, Cat.#: 11-5698-82), AF700 anti-Ki-67 (1:100, clone SolA-15, Thermo Fisher Scientific, Cat.#: 56-5698-82), PE anti-TCF1/TCF7 (1:40, clone S33-966, BD Biosciences, Cat.#: 564217), AF488 anti-pSTAT5 (0.03µg per test, clone 47/Stat5(pY694), BD Biosciences, Cat.#: 612598), eF660 anti-TOX (1:100, clone TXR10, Thermo Fisher Scientific, Cat.#: 50-6502-82), eFluor660 Rat-IgG2a-k isotype-control (1:100, clone eBR2a, Thermo Fisher Scientific, Cat.#: 50-6502-82), APC Mouse-IgG1k isotype-control (1:200, clone P3.6.2.8.1, Thermo Fisher Scientific, Cat.#: 17-4714-42), AF488 Mouse-IgG1k isotype-control (0.03µg per test, clone MOPC-21, Biolegend, Cat.#: 400132), and rabbit-anti-mouse-TCF1/TCF7 (1:100, clone C.725.7, Thermo Fisher Scientific, Cat.#: MA5-14965) followed by AF647 Donkey-anti-rabbit IgG (1:200, clone Poly4064, Biolegend, Cat.#: 406414) or DL488 Donkey-anti-rabbit IgG (1:200, clone Poly4064, Biolegend, Cat.#: 406416).

The following antibodies were used for cell hashing for scRNA-seq and scTCR-seq analyses:
BRAFV600E into Ptger2-/-Ptger4fl/fl: dilution: 1:250, TotalSeq-C 0302, clone: M1/42;30-F11, Cat.#: 155863, Biolegend
BRAFV600E into CD4CrePtger2-/-Ptger4fl/fl : 1:250, TotalSeq-C 0303, clone: M1/42;30-F11, Cat.#: 155865, Biolegend
BRAFV600E into GzmBCrePtger2-/-Ptger4fl/fl: 1:250, TotalSeq-C 0304, clone: M1/42;30-F11, Cat.#: 155867, Biolegend
BRAFV600E into WT: 1:250, TotalSeq-C 0301, clone: M1/42;30-F11, Cat.#: 155861, Biolegend

The following antibodies were used for in vivo depletion of T cells in mice:

Anti-mouse CD4 (100 µg/mouse, clone GK1.5, BioXCell, Cat.#: BP0003-1)

Anti-mouse CD8β (100 µg/mouse, clone 53-5.8, BioXCell, Cat.#: BE0223)

The following antibodies were used for in vivo blockade of IL-2 signalling in T cells:

Anti-mouse CD122 (300µg/mouse, clone TM-Beta 1, BioXCell, Cat.#: BE0298)

Anti-mouse CD132 (300µg/mouse, clone 3E12, BioXCell, Cat.#: BE0271)

If not stated otherwise, all antibodies were anti-mouse antibodies.

Validation

All antibodies listed in the previous section were validated by the manufacturer and/or by previous studies, and all primary antibodies were anti-mouse or anti-human antibodies. Mouse Cross-reactivity for anti-human antibodies was validated in-house using activation/stimulation assays in vitro with either mouse splenocytes or isolated CD8+ T cells from spleens.

Information on the validation of antibodies for flow cytometry can be found as stated below:

Biolegend antibodies: <https://www.biolegend.com/en-us/quality/quality-control>

Biolegend employs a comprehensive approach to antibody validation, analyzing 1-3 target cell types with single- and multi-colour analysis to encompass positive and negative cell types. Upon confirming specificity, each new lot is required to match the intensity of the in-date reference lot, with the brightness (MFI) evaluated across both positive and negative populations to ensure consistency. Furthermore, quality control testing, including a series of titration dilutions, is conducted for every lot.

Thermo Fisher Scientific antibodies: <https://www.thermofisher.com/de/de/home/life-science/antibodies/invitrogen-antibody-validation.html>

Thermo Fisher Scientific tests each antibody using different methods, including flow cytometry, Immunoprecipitation-Mass Spectrometry Antibody Validation, Knockout and Knockdown Antibody Validation, Independent Antibody Validation, Peptide Array Antibody Validation, Cell Treatment, Neutralization Antibody Validation, Relative Expression Antibody Validation, and SNAP-ChIP Antibody Validation. The precise validation method for each antibody is outlined in its respective antibody datasheet.

BD Biosciences antibodies: <https://www.bdbiosciences.com/en-eu/products/reagents/flow-cytometry-reagents/research-reagents/quality-and-reproducibility>

BD Biosciences tests each antibody on primary cells, cell lines or transfectant models using different methods, including flow cytometry, immunofluorescence, immunohistochemistry, or western blot. The precise validation method for each antibody is outlined in its respective antibody datasheet.

Validation and quality control of the TotalSeq-C 0301, TotalSeq-C 0302, TotalSeq-C 0303 and TotalSeq-C 0304 antibodies was carried out by Biolegend (<https://www.biolegend.com/en-us/quality/quality-control>) using flow cytometry (Cell-Surface Staining with Antibody: <https://www.biolegend.com/protocols/cell-surface-flow-cytometry-staining-protocol/4283/>) and sequencing as well as PCR to confirm the oligonucleotide barcodes (<https://www.biolegend.com/en-us/quality/quality-control>). Moreover, antibodies were validated in-house by flow cytometry using the PE anti-CD45 antibody (clone 30-F11, Biolegend, Cat.#: 103105) provided by Biolegend.

The anti-mouse CD4+ T cell-depleting antibody was validated by the manufacturer using western blot (<https://bioxcell.com>) and successful depletion was validated in-house by flow cytometric staining of CD4+ T cells.

The anti-mouse CD8+ T cell-depleting antibody was confirmed to deplete CD8+ T cells by Inge Verbrugge et al., Cancer Research, 2012 and additionally validated in-house by flow cytometric analysis of CD8+ T cells.

The anti-mouse CD122 blocking antibody was validated by Sultan, H., et al., Cancer Immunol Res., 2019 for successful in vivo blocking of CD122 signalling.

The anti-mouse CD132 blocking antibody was validated by the manufacturer using western blot (<https://bioxcell.com>) and successful in vivo blocking of CD132 signalling was validated by Y. W. He et al., PNAS, 1995.

Eukaryotic cell lines

Policy information about [cell lines and Sex and Gender in Research](#)

Cell line source(s)

Control BRAFV600E, Ptgs1/Ptgs2-/- BRAFV600E cell lines were sourced from the Immunobiology Laboratory at The Francis Crick Institute, London, UK. Their generation has been previously described (Zelenay et al., Cell 2015).

The cell lines BRAFV600E-OVA and Ptgs1/Ptgs2-/-BRAFV600E-OVA were generated by lentiviral transduction as described in the methods section).

D4M.3A-pOVA cells were generated as previously described (Di Pilato et al., Nature 2019).

MC38-OVA and Panc02 cells (commercially available from Cytion) were provided by Veit R. Buchholz (Institute of Medical Microbiology, Immunology, and Hygiene, Technische Universität München (TUM)).

MC38 (commercially available from Cytion) were provided by Achim Krüger (Institute of Experimental Oncology, TUM).

Authentication

For Ptgs1/Ptgs2-/- BRAFV600E cells, absence of PGE2 production was routinely confirmed by PGE2 ELISA (Cayman).

There were no further authentications conducted in the laboratory.

Mycoplasma contamination

All cell lines were routinely tested negative for mycoplasma contamination in-house by PCR.

Commonly misidentified lines (See [ICLAC](#) register)

No commonly misidentified cell lines were used in this study.

Animals and other research organisms

Policy information about [studies involving animals](#); [ARRIVE guidelines](#) recommended for reporting animal research, and [Sex and Gender in Research](#)

Laboratory animals

The following strains of mus musculus were used:
 Wildtype mice: C57BL/6J (strain #000664)
 OT-1 mice: C57BL/6-Tg(TcraTcrb)1100Mjb/J (strain #003831)
 CD45.1 mice: B6.SJL-Ptprca Pepcb/BoyJ (strain #002014)
 Ptger2^{-/-} mice: B6.129-Ptger2tm1Brey/J (strain #004376)
 Rag1^{-/-} mice: B6.129S7-Rag1tm1Mom/J (strain #002216)
 Ptger4fl/fl mice: B6.129S6(D2)-Ptger4tm1.1Matb/BreyJ (strain #028102)
 CD4Cre mice: B6.Cg-Tg(Cd4-cre)1Cwi/Bfl/J (strain #022071)
 GzmBCre mice: B6;FVB-Tg(GZMB-cre)1Jcb/J (strain #003734)

If not stated otherwise, all mice were used on a CD45.2/CD45.2 background. All mice were maintained and bred at the Klinikum rechts der Isar, Technical University of Munich, TUM or at the Klinikum der Universität München, Ludwig-Maximilians-University, (LMU) under specific-pathogen-free conditions. The following mouse strains were additionally bred by Charles River (Calco, Italy): Ptger2^{-/-}-Ptger4fl/fl, CD4CrePtger2^{-/-}-Ptger4fl/fl. Mice were housed under controlled conditions, including a 12-hour light-dark cycle, with an ambient temperature of 24°C, and humidity maintained at 55%. Mice were used at 6-12 weeks of age.

Wild animals

No wild animals were used in this study.

Reporting on sex

In all experiments, mice of the same age were sex-matched and randomly assigned to experimental and control groups. The results in this study are not restricted to one sex.

Field-collected samples

No field-collected samples were used in this study.

Ethics oversight

All mice were kept according to the guidelines of the Federation of European Laboratory Animal Science Associations and experiments were authorised by permission of the Government of upper Bavaria (Department 5).

Note that full information on the approval of the study protocol must also be provided in the manuscript.

Flow Cytometry

Plots

Confirm that:

- The axis labels state the marker and fluorochrome used (e.g. CD4-FITC).
- The axis scales are clearly visible. Include numbers along axes only for bottom left plot of group (a 'group' is an analysis of identical markers).
- All plots are contour plots with outliers or pseudocolor plots.
- A numerical value for number of cells or percentage (with statistics) is provided.

Methodology

Sample preparation

Cell isolation for flow cytometry and cell sorting:

Tumour or organ weight was determined using a microscale. Tumour samples were mechanically dissociated and incubated with Collagenase IV (200 U/ml) and DNase I (100 µg/ml) for 40 min at 37 °C and filtered through a 70 µm and a 30 µm cell strainer to generate single-cell suspensions. Spleens were passed through a 70 µm cell strainer, followed by red blood cell lysis and a second filtration step using a 30 µm cell strainer. Lymph nodes were passed through a 30 µm cell strainer. For the isolation of migratory cDC1, lymph nodes were processed as described for tumour samples.

For in vitro generation of repetitively activated TCF1+CD8+ T cells, naive splenic CD8+ T cells from WT mice were stimulated with mouse anti-CD3/CD28 microbeads and low dose IL-2 (85 U/ml) for two consecutive 48 h cycles. Cells were purified by gradient centrifugation (Pancoll) and used in experiments as indicated before staining with fluorescently-labelled antibodies in FACS buffer and flow cytometric analysis.

For further details, please see the methods section of the manuscript.

Instrument

Cells were analysed on a LSRFortessa Cell Analyzer (BD Biosciences) a SP6800 Spectral Cell Analyzer (SONY Biotechnologies) or a SA3800 Spectral Cell Analyzer (SONY Biotechnologies).

Naive CD8+ T cells were sorted using the SH800 Cell Sorter (SONY Biotechnology).
 Tumor infiltrating CD8+ T cells were sorted using BD FACSAria III Cell Sorter (BD Biosciences).

Reverse transcription of RNA into cDNA was performed using a ProFlex PCR System (Thermo Fisher Scientific).
 Quantitative real-time PCR was carried out on a LightCycler 480 (Roche).

Software	<p>The following softwares were used: SP6800 Sepctral Analyzer Software v2.0.2.14140 (SONY Biotechnology), SA3800 Spectral Analyzer Software v2.0.5.54250 (SONY Biotechnology), SH800 Cell Sorter Software v2.1.6 (SONY Biotechnology), BD FACSDiva™ Software v9.0.1 and v8.0.1 (BD Biosciences), LightCycler 480 SW v1.5.1 (Roche).</p> <p>All obtained data from flow cytometry was analysed with the FlowJo software (BD Biosciences, v10.8.1 and v10.8.2).</p>
Cell population abundance	<p>For the adoptive T cell transfers and scRNA sequencing + scTCR sequencing, respective cell populations were sorted using the "high purity" mode. Sorted fractions were assessed for purity and viability by flow cytometry. Purity of sorted naive and tumor-infiltrating CD8+ T cells was >95%.</p>
Gating strategy	<p>After gating on live, single cells, immune cell populations were defined the following:</p> <p>CD8+ T cells: CD45+CD8+TCRb+ or CD45+CD8+CD3+. Congenically marked cells were identified based on CD45.1/2 staining as indicated in the figure legends. T cell subpopulations were identified using the following additional markers: CD44, TIM-3, CXCR6, TCF1, CD62L, TOX, Ki-67, and GzmB</p> <p>CD4+ T cells: CD45+CD4+TCRb+</p> <p>Migratory cDC1 in tdLN: CD45+CD11c+MHCIhiCD103+CD8a-CD11b-</p> <p>In vitro generated repetitively stimulated TCF1+CD8+ T cells: CD45+CD8+TCRb+ or CD45+CD8+CD3+</p> <p>Naive OT-I T cells from blood for adoptive T cell transfers: CD45.1+CD8a+CD62L+CD44low</p>

Tick this box to confirm that a figure exemplifying the gating strategy is provided in the Supplementary Information.